



LAWRENCE  
LIVERMORE  
NATIONAL  
LABORATORY

# National Ignition Facility Laser System Performance

M. Spaeth, K. Manes, M. Bowers, P. Celliers, J. M. Di Nicola,  
P. Di Nicola, S. Dixit, G. Erbert, J. Heebner, D. Kalantar, O.  
Landen, B. MacGowan, B. VanWanterghem, P. Wegner, C.  
Widmayer, S. Yang

August 5, 2014

Fusion Science and Technology

## **Disclaimer**

---

This document was prepared as an account of work sponsored by an agency of the United States government. Neither the United States government nor Lawrence Livermore National Security, LLC, nor any of their employees makes any warranty, expressed or implied, or assumes any legal liability or responsibility for the accuracy, completeness, or usefulness of any information, apparatus, product, or process disclosed, or represents that its use would not infringe privately owned rights. Reference herein to any specific commercial product, process, or service by trade name, trademark, manufacturer, or otherwise does not necessarily constitute or imply its endorsement, recommendation, or favoring by the United States government or Lawrence Livermore National Security, LLC. The views and opinions of authors expressed herein do not necessarily state or reflect those of the United States government or Lawrence Livermore National Security, LLC, and shall not be used for advertising or product endorsement purposes.

## **NATIONAL IGNITION FACILITY LASER SYSTEM PERFORMANCE**

Mary L. Spaeth, Kenneth R. Manes, M. Bowers, P. Celliers, J-M. Di Nicola, P. Di Nicola,  
S. Dixit, G. Erbert, J. Heebner, D. Kalantar, O. Landen, B. MacGowan, B. VanWanterghem,  
P. Wegner, C. Widmayer, S. Yang

All with Lawrence Livermore National Laboratory

### **ABSTRACT**

The National Ignition Facility (NIF) laser is the culmination of more than 40 years of work at Lawrence Livermore National Laboratory (LLNL) dedicated to delivery of laser systems capable of driving experiments for the study of high-energy-density physics. Although NIF has been dedicated to supporting a number of missions, it was clear from the beginning that its biggest challenge was meeting the requirements for pursuit of Inertial Confinement Fusion (ICF). Meeting the NIF Project Completion Criteria in 2009 included meeting a large portion of the NIF Functional Requirements and Primary Criteria that were established for the Project in 1994. During the National Ignition Campaign and as NIF transitioned to a user facility, its goals were expanded to include requirements defined by the broader user community as well as laser system designers and operators.

Keywords: NIF Laser, Laser Fusion, ICF Laser

This work is performed under the auspices of the U.S. Department of Energy by Lawrence Livermore National Laboratory under Contract DE-AC52-07NA27344.

LLNL-JRNL-658064

## **I. AN OVERVIEW FOR MEETING THE NATIONAL IGNITION FACILITY AND NATIONAL IGNITION CAMPAIGN PROJECT GOALS**

Between 1993 when the National Ignition Facility (NIF) laser was being designed<sup>1</sup> and 1997 when construction began, the long-term goals for NIF performance were established and documented as the Functional Requirements and Primary Criteria (FR&PC). The latest update of the FR&PC is Revision 1.8.<sup>2</sup> There were no changes regarding laser performance between the original and the most recent revision. Foremost among these requirements is the need to deliver 1.8 MJ to experimental platforms or “targets”. Handling a large amount of energy is inherent in meeting the NIF missions. Because igniting fusion fuel requires stellar temperatures and densities, NIF must precisely compress energy in time and space for this purpose. Fusion experiments currently (April 2014) underway in NIF deliver x-ray burn widths of ~150 ps.<sup>3</sup>

During NIF construction and commissioning, Project goals were expressed in terms of milestones for cost, schedule, intermediate hardware performance status, and risk. In 2009, “Project completion” for the laser was judged by its ability to meet its formal Project Completion Criteria (PCC).<sup>4</sup> This included (1) measurements made for its Performance Bundle, B14, (2) operation of half of the beamlines at half of their design power and energy, and (3) acknowledgement that it was well on its way to meeting the full FR&PC. As seen in Table I, many of the FR&PCs were already met by the time of Project completion. By the end of the National Ignition Campaign (NIC) in 2012, NIF had been ramped up to full power and energy, as demonstrated by the shot on July 5, 2012, with an energy greater than 1.8 MJ (1.86 MJ) and power above 500 TW (523 TW).<sup>5</sup>

Most of the laser FR&PCs were evaluated by direct measurement of NIF’s full system performance. However, two were evaluated using a combination of measurements and

calculations: laser spot size and laser pre-pulse. Laser spot size was measured for one beamline, a beamline that was redirected to the precision diagnostic system (PDS) where a broad suite of laser diagnostics was available.<sup>6</sup> Although not required by Project completion requirements, confirming measurements have been made for the spot size of beams across the full NIF (see Section II.J Laser Spot Size). Laser pre-pulse was not directly measured at Target Chamber Center because of the fierce environment that would be encountered by a detector placed at this location; instead, pre-pulse was projected on the basis of calculation and other measured laser parameters.<sup>7</sup>

The most important requirement for the NIF laser was that it be safe—safe to build and safe to operate. Keeping NIF personnel and its machine equipment safe has at all times been of highest priority to the NIF team during construction, testing, and now operation of the laser. The need for NIF to be an energy-in-time compressor forces it to be a big laser, able to handle a large amount of energy. Being this big brings with it potentially hazardous conditions, all of which must be mitigated with very high confidence. The following discussion provides a sense of the potential hazards by keeping in mind that a hand grenade typically releases a little over half a MegaJoule (MJ) of energy.

NIF energy-in-time compression is accomplished by a series of steps from the wall plug to the target. The energy requirements build up because some of these steps are rather inefficient. The first step is accumulation of ~400 MJ of energy from the utility power line over a time frame of ~2 minutes. This energy is stored in capacitors that are held at ~20,000 volts located within the metal housings of its power-supply modules.<sup>8,9</sup> The charging process involves relatively conventional conversion to 20-kV DC, but the energy density reached in oil-filled capacitors is uncommonly high. The capacitors release the 400 MJ in about half a millisecond to the

flashlamps that surround laser slabs, delivering energy optically to the neodymium-dopant in the glass. Transfer of energy from the flashlamps to the slabs has relatively low efficiency. The xenon-filled flashlamps expend most of their energy reaching a blackbody temperature of  $\sim 10,000^{\circ}\text{C}$  with significant energy going into the creation of mechanical and thermal shocks to the amplifier structure. The Nd ions store a fraction of this energy for  $\sim 0.5$  ms and then release a little more than half of it to the propagating laser beams in a time frame that is typically 3–15 ns.

As the lasers propagate through their beampaths they each develop a spatial intensity profile structure that could harm downstream optics.<sup>10</sup> Much of this structure can be filtered out by focusing the beams through “pinholes” sized from 0.2- to 1-cm diameter. Because a laser of this energy cannot be focused to this small size in air, the pinholes are housed in evacuated structures called “spatial filters”. The energy in one of the laser beams, should it break into one of its non-linear operating regimes, has the potential to break a spatial-filter lens, the vacuum barrier for the spatial filter. If a person were near a window of one of the spatial filters when it happened to break, the subsequent event would be very similar to sitting next to a breaking window in an airplane (quite often accurately displayed by the film industry). The energy associated with the rapid pressure rise (rupture) of a single spatial filter would be  $\sim 9.5$  MJ. All large evacuated structures pose a similar hazard.

After leaving its last spatial filter, a beam propagates through a (nearly evacuated) Final Optics Assembly (FOA) and into the 10-m-diameter evacuated target chamber. The next relatively low-efficiency step is compression of the target. As the beams hit an Inertial Confinement Fusion (ICF) target the  $\sim 15$ -ns laser pulses compress the target to the point where it can give up its energy in a time frame (as of today) of little more than 100 ps. Overall, the time intervals involve a range from  $\sim 2$  minutes to  $\sim 100$  ps, a time compression factor of  $\sim 1 \times 10^{12}$ .

Many steps along this path have the potential to be lethal. The NIF has implemented a great number of engineering and procedural techniques for mitigating these and many more of the hazards that accompany such a large laser. Some of the most notable are fail-safe circuits in the Master Oscillator Room (MOR) to keep the laser from entering one of its potentially non-linear modes;<sup>11</sup> argon along the beampath from the last spatial filter to the final optics to avoid another possible non-linear regime;<sup>12</sup> rupture panels on top of all spatial filters (should a vacuum barrier ever break, the pressure pulse would be directed upward into a region where people are not allowed); totally enclosed laser beampaths; and keep-out rules that disallow the presence of personnel in the capacitor bays, laser bays, switchyards, and target bay during a shot. Keeping personnel out of the switchyards and target bay protects them from hard x-rays produced by almost every NIF shot as well as from light that might have escaped from its enclosure. Large, heavy, radiation- and neutron-shielding doors for the target bay are closed whenever the maximum credible yield for a shot is over  $10^{14}$  neutrons (now often done), and similar doors for the switchyard are closed if the maximum credible yield for a shot is over  $10^{16}$  (becoming more common).

The safety of all personnel associated with the construction of NIF was also given very high attention by NIF management and supervisory personnel. No steps were taken without very conscious decisions ensuring they could be completed without risk to personnel. As a result the safety record of the NIF construction team was exemplary, receiving an award from the National Safety Council for more than 5 million man-hours of work without a lost-time injury.

No team can ever rest on its safety laurels. Attention to safety continues to be kept high. Safety-conscious practices, both for personnel and for the machine, have continued as NIF now operates as a user facility. Formally, the NIF laser has met and continues to meet all of its safety

requirements as specified in the NIF FR&PC that conform to the American National Standards Institute (ANSI) Z136.1.

## **II. CATEGORIES OF NIF CAPABILITIES**

### **II.A Laser Energy and Peak Power**

The first two items on the list of Primary Criteria, “laser energy and peak power”, specified that the laser be capable of routinely delivering a temporally shaped pulse with energy of at least 1.8 MJ and a peak power of greater than 500 TW to Target Chamber Center. Both of these requirements were first met simultaneously on a shot taken on July 5, 2012. The power as a function of time within the pulse for the July 5 shot is shown in Fig. 1; the energy delivered was 1.86 MJ. Laser power exceeded 500 TW (measured at 523 TW) as can also be seen in Fig. 1. Calibration of the energy measurement detectors was traced through a secondary standard back to a primary standard held by the National Institute of Standards and Technology (NIST).

The nomenclature for referring to different features of an ICF laser pulse that will be used several times in this document and elsewhere in this special issue of FS&T is illustrated in Fig. 2. Not all ICF shots have the same number of shocks,<sup>3</sup> in which case a similar nomenclature applies. The foot of the pulse refers to the time interval between the very beginning of the pulse up to the time when the pulse for the last shock just begins to rise. Other terms can also be seen in the figure.

#### ***II.A.1 Delivering $3\omega$ Energy and Power***

The NIF system is able to deliver a total of 1.8 MJ and 500 TW peak power to target chamber center (TCC) in a 3-ns, damage-equivalent pulse length<sup>13</sup> because each of its 192 beams can deliver its proportional share of these values. Flexibility has been designed into the laser for

providing energy and power over a wide range of operating parameter space, as collectively described by Fig. 3. Power-vs-energy relationships are plotted for both the performance of individual beams and the collective behavior that can be expected for the full system. These power-vs-energy diagrams have been a metric for NIF laser performance since it was first being designed.<sup>1</sup> In Fig. 3, three curves for the full system are overlaid on the plot of performance for individual beams. The two solid-line curves indicate the limits for two examples of laser pulse shapes, one for a square pulse called flat-in-time (FIT) and one for the type of shaped pulses that are typical for ICF users. In this plot the upper power for FIT pulses is set by filamentation damage that would be expected to occur very early in the pulse when the gain saturation of the  $1\omega$  amplifiers is low and the resulting  $3\omega$  spatial contrast across the beam is high.<sup>14</sup> Filamentation would occur at locations where the local intensity is high even though the spatially averaged intensity is considerably lower. At the upper end of the energy range the FIT curve turns over, first due to a  $1\omega$  damage limit for the polarizer and at higher energy because the regenerative amplifier at the input to the laser chain has run against its energy-delivery limit. At high energy there are several other effects that are setting in at about the same place: the power amplifiers are reaching their design point for stored energy received from the flashlamps, and the performance of the frequency-conversion crystals rolls over because as the peak power drops, the efficiency of the frequency converters also falls.

Similar but less constraining power limits exist for the peak of a shaped pulse. Near the end of these pulses when the average intensity of the beam spatial profile is high, gain saturation in the  $1\omega$  amplifiers has already occurred and local variation of the intensity relative to average is lower. The shaped-pulse-limit curve has annotations that identify the equivalent Gaussian width of the shaped pulse as calculated by the Equivinit<sup>13</sup> algorithm.

The set of data points on the left edge of Fig. 3 and identified as impulses are for short, 88-ps, full-width-at-half-maximum pulses.

Damage initiation and growth on  $3\omega$  fused-silica optics<sup>15,16</sup> also limit the space over which the laser can be operated, as shown by the dotted curve set by the capacity of the “NIF Optics Recycle Loop” described in this issue of *FS&T*. The curve shown in Fig. 3 is based on a recycle rate of 40–45 optics per week. Recall that it is the Optics Recycle Loop that allows the NIF laser system to operate routinely above the damage growth limit.

All of the data in Fig. 3 are given for the system as it is fully configured as an ICF driver, that is, with its full complement of beam-smoothing, diagnostic, and machine-protection equipment. This includes the Continuous Phase Plates (CPPs), polarizers, grating debris shields, and disposable debris shields (DDS).

Figure 4 shows the history of full-system output energy delivered by NIF as a function of time after completion of the NIF Project and throughout the National Ignition Campaign. The flexibility of the Optics Recycle Loop allows scheduling of requested experimental shots while staying within the limitations of the optics-use budget. For example, trade-offs can be made between the operating points (energy and power) of individual shots and the number of shots that can be taken over a defined time interval.

## **II.B Capsule Irradiation Symmetry**

As described in “Description of the NIF Laser”, also in this issue of *FS&T*, the top-level architecture of the entire facility (including the laser bays, switchyards, and target bay) was selected to meet the capsule irradiation symmetry requirement. As summarized in Fig. 5, eight-fold symmetry has been provided in four cones of laser quads (a quad represents four beams

coming from one laser port on the target chamber). The inner-cone quads are located at nominally 23.5 and 30 degrees, as measured from the poles of the target chamber, and the outer cone quads are located at 44.5 and 50 degrees. The NIF beams are currently arranged to support vertically oriented, indirect-drive hohlraum targets. The different cones and sets of quads are shown (online in color) in Fig. 5 and discussed in more detail in Section II.C.1.

## **II.C Laser Wavelength**

The primary criterion that the output wavelength of the laser be 0.351  $\mu\text{m}$  is met on every shot. Frequency conversion components that sit within the FOAs positioned just before the beams enter the target chamber receive high-energy, high-power beams from the near-IR laser amplifier chains and deliver a near-UV wavelength to the target. The accuracy of the 0.351- $\mu\text{m}$  wavelength is established by the accuracy of the fundamental wavelength. The wavelength of the 1.053- $\mu\text{m}$  light, measured with a commercial WA-1650 EXFO (formerly Burleigh) wavemeter, has proven to be very stable with temperature control only. A portion of a wavelength stability measurement made from June of 2005 to November of 2006 is shown in Fig. 6. As seen from this figure, the goal for wavelength stability that was set as a sub-system requirement has been significantly exceeded.

### ***II.C.1 Wavelength Tuning***

During writing of the *Laser Design Basis for the National Ignition Facility*<sup>1</sup> in 1992 and 1993, target designers often requested the availability of more than one  $\sim 0.351\text{-}\mu\text{m}$  wavelength on target (the third harmonic of the 1.053- $\mu\text{m}$  fundamental laser wavelength). Wavelengths considered were those that could be generated within the bandwidth of the 1.053- $\mu\text{m}$  transition in Nd:glass. Because continued analysis indicated that a multiple-wavelength capability would be

necessary for exploring the range of interest for the ICF mission,<sup>17,18,19</sup> the as-built NIF laser is capable of delivering the 0.351- $\mu\text{m}$  light at three individual wavelengths separated by up to  $\sim 3$  Angstroms. The colors of the quad sets shown (online) in Fig. 5 indicate the availability of three individually tunable wavelengths, over  $\sim 9.6$  Angstroms at  $\sim 1.053 \mu\text{m}$  that are currently available as a tuning choice for target designers. In the current NIF configuration, three different master oscillators, each with a different color, are set up to drive the different cones of quads in NIF. The outer cones are typically (circa 2014) set to a shorter wavelength than the inner cones, and the  $30^\circ$  quads are often setup to have a slightly shorter wavelength than the  $23^\circ$  quads. These relationships were established for support of cross-beam energy transfer from outer to inner and from  $30^\circ$  to  $23^\circ$  beams in pursuit of improving the symmetry of ICF capsule convergence.<sup>20</sup>

Although 3 individual wavelengths can be generated in 3 individual,  $1\omega$  master oscillators, delivery of light to the target over a range of wavelengths is possible only if predictable gain can be produced all along each full amplifier chain over the entire range of tunability. Because 116 rod passes (57 cavity passes  $\times$  2 passes through the rod for each pass, plus 2 additional rod passes during the partial round trip as the beam enters and exits the cavity) are made within the regenerative amplifiers, these pre-amplifiers are the most wavelength-sensitive elements in the chains. In order to meet the challenge of tuning from one wavelength to another “on a routine basis”, it was necessary to flatten the gain profiles of these dispersion-sensitive components. The ability of the regenerative amplifiers to preserve their output-energy performance over a bandwidth of  $\sim 20$  Angstroms (at  $1\omega$ ) is shown in Fig. 7. The values of the wavelengths shown in this figure are those that were used by the laser on July 25, 2013, although tuning over an  $\sim 9.6$ -Angstrom bandwidth is done on a regular basis. The limit of the NIF tuning range is not only set by the bandwidth of the regen amplifier; limits of the geometry of the beam

dump for the frequency-tripling crystals also have an impact. Folding together the tuning ranges of the regen and management of back-reflected light from the tripler crystals results in an overall NIF  $1\omega$  tuning range of  $\sim 9.6$  Angstroms.

## **II.D Laser Pulse Dynamic Range**

As originally defined the functional requirement for the pulse dynamic range, the ratio of the peak power of the pulse compared to the minimum power in the trough, was required to have a peak value of at least 50:1. At the time of NIF Project completion, target designs had evolved, and as a result the requested and then demonstrated pulse dynamic range over an ICF pulse shape had increased from greater than 50:1 to 176:1. Subsequent to Project completion, as target designers continued to refine the desired ignition-point design target, the corresponding desired pulse dynamic range for the laser moved upward again. By the end of the NIC Program, target designers were setting requested pulse dynamic range values of greater than 300:1. Figure 8 provides the measured pulse shape and the dynamic range realized for the same July 5, 2012, shot described in Section II.A.

As seen in Fig. 8, the dynamic range for the July 5, 2012 shot was greater than 300:1 for the duration of the trough, very significantly better than originally specified.

## **II.E Beamlet Power Balance**

Power balance for the NIF laser system is a measure of the quad-to-quad laser-power uniformity in the context of the output power of the entire laser system. Because NIF pulse shapes can have very fast rise times, on the order of  $\sim 100$  ps, a flowdown requirement for the simultaneity of the beginning of the pulse from each beamline was needed and established. Thus the goal for 30-ps rms simultaneity is interpreted as a subset of the requirement for power

balance. Early in the NIC Program we learned that streak cameras would not achieve the required  $\sim 10$ -ps measurement accuracy across all 192 beamlines simultaneously. In response, a new procedure for measuring pulse synchronization was developed. This procedure uses amplification of a short ( $\sim 88$  ps) impulse from the master oscillator, by only the regenerative amplifier, for one beam at a time, with arrival times measured at two different locations along the beamline on the same shot. The impulse is shaped by the Amplitude Modulation Chassis (AMC) in the Master Oscillator Room (MOR) for the quad of that beamline. As described by Fig. 9, the procedure measures arrival of the impulse at the output of the regenerative amplifier (as collected in the Input Sensor Package (ISP)) and at target chamber center (TCC). More details about the MOR and the ISP are given in the “Description of the NIF Laser”, this issue of *FS&T*. A similarly short optical timing fiducial pulse (called FIDU) is also produced in the MOR and passively split to provide input to all high-speed diagnostics in the facility, including those for target performance as well as those assigned to the laser. The AMC and FIDU systems are both instructed to provide their output pulses by the NIF Master Timing System.

The light reaching TCC is collected by the pulse-synchronization target pictured in Fig. 10. This target has top and bottom diffusers capable of accepting the corresponding input from beams in either the top or the bottom hemispheres of NIF.

An aspheric lens is located behind each diffuser to couple the light from that diffuser into its own dedicated optical fiber. The two fibers, one each for the top and the bottom diffusers, are used one at a time to carry light to 12-GHz detectors (Newport model 1544-A-50) and then to Channel 1 or Channel 2 of a fast scope (with 40-ps time samples). Fiducial light for comparison to the TCC impulse is routed to a Terahertz Technologies 10-GHz optical detector and then to Channel 4 of the same fast scope. During a pulse-synchronization test, 10 shots are recorded for

every beamline, starting, for example, with B115 and continuing through all of the beams in the corresponding hemisphere. Completion of this series of tests for one hemisphere takes about 3.5 hours. For each of the 10 shots per beamline, the difference in the time of arrival of the fiducial pulse and the laser impulse is recorded at both sampling locations, at the ISP and TCC. The ISP data is used to back out any shot-to-shot variances in the master oscillator system. Calculation of the rms timing error derived from these measurements begins with calculation of the timing error for an individual shot:

$$\Delta T_i = [(T_i - T_{ref})_{TCC} - (T_F - T_{Fref})_{TCC}] - [(T_i - T_{ref})_{ISP} - (T_F - T_{Fref})_{ISP}]$$

where  $T_i$  and  $T_F$  (identified in Fig. 9) are the measured times of appearance of the impulse and the FIDU signals in the scope traces, and  $T_{ref}$  and  $T_{Fref}$  are their corresponding expected times for appearance. The error in identifying the locations of the individual fiducial and laser impulse signals along the scope traces is typically  $\sim 2$  ps. After corrections of known offsets, the rms timing error for each beam, derived from the measurements taken during the 10 shots is then:

$$\Delta T_{rms} = \sqrt{\sum_{i=1}^{10} \Delta T_i^2}$$

This equation explicitly does not include the jitter in the MOR pulse shaping system. It includes only the static portion of the timing errors at Target Chamber Center (TCC). The dynamic portion is monitored on every rod shot and system shot by analysis of the actual arrival time of the laser pulse at the ISP Power Sensor compared to its expected arrival time. The expected arrival time of the laser pulse is calculated from the measured arrival time of the FIDU pulse. The results of these measurements are recorded by the Laser Performance and Operations

Model (LPOM) and can be added in quadrature to the term given above to find the complete timing error. (See Section IV of “Description of the NIF Laser”, also in this issue of *FS&T*, for more discussion of LPOM.)

Figure 11 contains a histogram for a pulse-synchronization test conducted in April of 2012. The relative timing error for all beamlines compared to one common reference time after accounting for known offsets was  $\sim 10$ -ps rms. Two such tests were performed 18 months apart, finding that half of the NIF beams had the same offset as they did on the first test to within 10-ps rms and the rest had offsets that fell to within 15-ps rms. Slow drift in the AMC response is now corrected on a monthly basis to compensate for this possible source of timing error.

Finding the timing error for full-system shots includes comparison of the starting point for each shaped (not-impulse) laser pulse to the temporal location of the common FIDU pulse. For full-system shots the NIF Master Timing System provides electronic triggers to multiple subsystem within NIF, including triggers for the AMCs for each quad and triggers for all high-speed temporal diagnostics, such as for the diagnostics of the  $1\omega$  pulses going through each pre-amplifier and amplifier section of the laser chains and for the diagnostics for the optical FIDU. The ISP diagnostic now becomes the reference that links the time at TCC measured during the pulse-synchronization measurements and the time measured on system shots. The 50% amplitude point on the first rising portion of each shaped pulse is designated as  $t = 0$  for that pulse, and the error between where this point is found and where it was expected with respect to the fiducial pulse is reported for each shot by the LPOM. Several contributions to the temporal error are then rms-added to calculate a timing uncertainty for each full system shot. The small uncertainty in locating the fiducial pulse is combined with the 10-ps synchronization error described above and the uncertainty in locating the  $t = 0$  point of the shaped pulse. Although the  $t$

= 0 point measurement uncertainty is different for different pulse shapes, the overall rms pulse-timing error for the range of pulse shapes encountered remains less than 30-ps rms (typically) compared to the requested timing.

The power-balance requirement for an ignition pulse has evolved in time consistent with the evolution of the ignition-point design target and its corresponding laser pulse shape. This evolution began in 1992 during preparation of the NIF Laser Design Basis document;<sup>1</sup> it continued through the Rev 0 to Rev 5 ignition-point designs and continues today.

Power balance is the variance of the individual “quad” power profiles relative to the “average” value of the power for a common pulse shape as box-car averaged over 2-ns time intervals. It is defined by cone for a common pulse shape and with a box-car average with a 2-ns time interval, as described by the equation shown in Fig. 12.

In this equation  $n$  is the number of quads with the same pulse shape,  $P_i^{sm}$  is the 2ns-smoothed  $3\omega$  power measurement of the  $i^{th}$  quad, and  $\bar{P}_{cone_i}^{sm}$  is the average of all 2ns-smoothed power measurements within the cone of the  $i^{th}$  quad. Note that, as described later in section II.N, for each quad the  $3\omega$  power is calculated based on a direct measurement of 1 beamline, the flow-forward calculated power for 2 beamlines with a direct measurement of the  $1\omega$  pulse shape, and the flow-forward calculation of the 4th beamline from the injected-laser pulse shape. All 4 beamline powers are normalized to their independent direct  $3\omega$  energy measurements. Target interactions with the laser, such as the symmetry of the beams within the hohlraum, the pointing of the laser beams with respect to the hohlraum, clipping of the beams by the LEH, or any other asymmetries of the target that might exist are not considered when evaluating power balance performance.

At the end of the NIC Program, as a Rev 5 ignition-point design was being studied, laser power balance was also evaluated for the shot taken July 5, 2012 and is shown in Fig. 13. The laser pulse shape was the Rev 5 ignition-point design pulse. The dotted line in Fig. 13 shows the specification for power balance for this pulse shape. The power-balance requirement is different for different parts of the pulse, being 12% rms in the picket, 20% rms in the trough, and 3% rms during the peak of the pulse. The green line (shown in color in the online article) is the power balance achieved for the July 5 shot for the full laser system as calculated from all measured quad parameters; it represents the observed value of power balance for NIF, meeting the requirement at all points along the time line of the pulse. Note that the higher the laser pulse dynamic range, discussed in the previous paragraph and above 300 for this shot, the more difficult it is to meet the power-balance requirement during the period of the trough. Thus NIF now provides a power-balance capability far more stringent than its original requirement.

## **II.F Beamlet Positioning, Pointing Accuracy**

The pointing requirement is one of a set of requirements intended to assure radiation symmetry sufficient for achieving the implosion symmetry needed for ICF capsules. Pointing accuracy for NIF was first measured as part of the PCC for the first 96 beams (from Laser Bay 2, 48 beams from the top hemisphere and 48 from the bottom). The PCC requirement reads, “the beam pointing accuracy shall be less than or equal to 100  $\mu\text{m}$  rms in the target plane”. Beam positioning accuracy was demonstrated in January of 2009 by recording the x-ray emission from 96 beams incident on a gold-coated silicon target. The measurements show  $<64 \pm 4 \mu\text{m}$  rms beam-to-target positioning accuracy for 96 beams on NIF shot N090114-002-999.

The pre-NIF era of ICF lasers at Lawrence Livermore National Laboratory (LLNL) provided very important background experience for designing the very stable platform needed

for precision alignment. First, the building itself was designed to minimize its response to sources of vibration. Second, the optical system was designed to minimize beam motion in response to vibration of the building.<sup>21</sup> All of the optical components are located on a large, thick concrete “optical table” that is mechanically isolated from the rest of the conventional facility. Heavy, rigid support structures are provided for the optical components residing on this optical table. Engineering of the details for coupling the space frame that supports the heavy transport mirrors in the switchyard to the building structure were given special attention. Finite element analysis of vibration modes that could be supported by each of the refractive and reflective optical components was used to guide design of their alignment and support structures. Temperature-control systems that can achieve plus/minus quarter-degree-Celcius temperature accuracy were provided for the laser bays, the switchyards, and the target bay. Temperature control inside the FOAs is even tighter at plus/minus  $\sim 0.05^{\circ}\text{C}$ . The beam alignment process, completed in terms of target chamber coordinates, traces its accuracy back to a network of survey markers located throughout the laser and target areas.<sup>22</sup>

The strategy for determining the beam-positioning accuracy on NIF includes a combination of continuous wave (CW) alignment tests, rod shots to the Target Alignment Sensor (TAS), and target shots for final validation.

The TAS, shown in Fig. 14 (a) and 14 (b) is the device that enables beam pointing and target positioning.<sup>23,24</sup> This system is positioned at TCC with the TAS positioner. The target is inserted into the TAS and held by the target positioner as seen in Fig. 14 (a). The TAS incorporates two mirrors and four CCD sensors to view and align both the beams and the target. Each of the upper and lower TAS assemblies or jaws incorporates a mirror, a lens, and two CCD cameras. Together these components allow measurement of each beam with respect to the target

position. This information is the feedback used for closed-loop alignment of the beams by angular adjustment of the transport mirrors. The jaws are mounted on stages that can open and close to accommodate different-sized targets. A photograph of the TAS in the target chamber of NIF is shown in Fig. 15.

The strategy for target and beam alignment includes the following:

- Offline calibration and online validation of the TAS for referencing the view of upper beams relative to the target and lower beams relative to the target; the upper and lower views relative to each other and to the internal TAS coordinate system (part of initial set-up and qualification).
- The Chamber Center Reference System (CCRS) that unambiguously establishes the location of TCC. During target alignment, TAS is positioned at TCC as viewed by the CCRS, where it becomes the secondary reference for locating the target and for aligning the beams with respect to the target (every shot).
- Rod shots to the TAS that are used in NIF to measure the alignment between the CW alignment beams and the pulsed beams and to adjust the CW alignment light source of each beam to match the pulsed beam on target (verified occasionally).
- Beam-to-target positioning that is validated with target shots using a thin flat target. X-ray spots generated by the incident NIF beams are compared to the expected locations to quantify the alignment accuracy (verified occasionally).

The flat, thin target is a gold-coated silicon plate. To meet the NIF Project Completion Criteria, 48 top-hemisphere laser beams were pointed to specified locations on the top side of the plate. Another 48 laser beams from the bottom hemisphere were pointed to specified locations on

the bottom side of the plate. There is no bleed-through of x-rays generated by these lasers from one side of the plate to the other. Small fiducial holes are etched through in the target plate at locations that are visible by the TAS and well known in the TAS coordinate system. X-rays generated by illumination of these fiducial holes by beams on one side of the plate can be seen by a detector on the other side of the plate. These holes and their x-ray images are used to calibrate measurement of the locations of all of the beams with respect to TAS and thus with respect to the target.

The diagnostics for the x-ray measurement are 2 Static X-ray Imagers (SXI) used with the shortest laser pulses available from NIF (88-ps impulses, see Section II.H.1) to minimize hydrodynamic blurring on the integrated target image. One SXI measures the 48 beam positions from the upper surface of the target and the other measures the locations of the 48 beams hitting the lower surface. There were an additional 6 beams (2 on the top surface and 4 on the bottom surface from beams beyond the first 96) that illuminated holes and provided the absolute positioning references described above. Figures 16 (a) and (b) show the x-ray images of the 96 beams used to measure pointing error, along with images of the 6 fiducial beams as they were recorded by the 2 SXI diagnostics. The beams used to illuminate the target registration fiducials are indicated with box outlines. These beam spots are not included in the analysis. Note that the circled images of x-rays from the fiducial holes correspond with the images of their illuminating lasers, seen in the square boxes on the opposite side of the target plate.

After the shot, the SXI images were analyzed to measure where the beams hit relative to the fiducial holes in the target and with respect to the TAS coordinates. The TAS images of the final target alignment in the target chamber provided an accurate reference for the target fiducials. The SXI images were oriented and scaled to target chamber coordinates using the

locations of the fiducial spots compared to the TAS images of the target. The locations of the x-ray spots were then calculated and compared to the beam aim points. With this combination of data, the locations of where the beams hit in terms of TAS coordinates could be calculated. The analyzed data is also shown in Fig. 16.

Uncertainty in the pointing measurement was estimated by evaluating systematic errors. Different analysis techniques were in agreement to within  $\pm 3 \mu\text{m}$ . This included uncertainty in identifying the peak location of any beam spot and uncertainty due to magnification error that was found to be  $\pm 2 \mu\text{m}$ . This was based on the accuracy of the spacing of the fiducial holes and the spacing of images recorded from multiple pinholes compared to offline measurement of the pinhole spacing. The combined uncertainty was found to be  $\pm 4 \mu\text{m}$ .

During NIC, improvements in pointing accuracy were made as experience was gained in using TAS and the procedural steps used for achieving alignment. Figure 17 illustrates the improvement demonstrated with a shot on April 27, 2011. In that shot 62 beams were measured on target, and the result indicated a pointing accuracy of  $38 \pm 4 \mu\text{m rms}$ , meeting the original requirement of  $<50 \mu\text{m rms}$ .

## **II.G Direct-Drive Requirements**

One of the Primary Criteria for NIF is that the possibility for Direct-drive ignition experiments not be precluded.<sup>25</sup> Several features of NIF have been designed to be consistent with this mission.

The NIF target chamber was designed with laser entry ports near the equator at locations specified for Direct-drive FOAs. The locations of these ports were selected to provide spherical target illumination for a Direct-drive target and can be seen as available for use in a photo of the

NIF target bay given in Fig. 18. The 2-m-thick concrete shielding walls around the target bay also include appropriate openings for delivery of the Direct-drive beams. Switchyard space frames, mirror mounts, and beam tubes have also been fabricated to be adapted for the Direct-Drive mission.

Direct-drive targets require a larger and more complicated spectral bandwidth than indirect-drive targets. Space has been reserved in the regenerative amplifier housings of the Injection Laser System (ILS) for modulator components that could be requested for generation of this bandwidth during pre-amplification of direct-drive laser pulses. More information on the ILS is given in “Description of the NIF Laser”, also in this issue of *FS&T*.

In addition, the design of the NIF FOAs includes a slot not used for indirect-drive experiments but is available for holding an additional tripler of specific interest for direct-drive users; the additional crystal is designed to widen the bandwidth for frequency conversion to  $3\omega$ . At the time of the final design of the FOAs, target designers of direct-drive experiments defined the need for 2 triplers rather than the 1 used by indirect drive to enable the broader spectral line width they calculated would be required by a direct-drive target.

## **II.H Laser Pulse Duration**

The original requirement for laser-pulse duration for NIF was  $\geq 20$  ns. Several features of the laser design have a potential for limiting the pulse length. Features that are now *not* limiting include (1) the  $1\omega$  main amplifier does not limit the pulse length, it could support a pulse length as long as  $\sim 100$  ns, (2) pinhole closure in the spatial filters also does not limit pulse length because pinholes are held at  $\sim 10^{-4}$  Torr, and (3) because no high-intensity ghosts (in an

atmosphere above  $\sim 10^{-4}$  Torr) are allowed to form on axis, an air or argon spark created by the front end of a long pulse cannot bite off the back end of that same pulse.

The maximum pulse length that can be delivered from the ILS to the  $1\omega$  main amplifiers is determined by the design and physical path length of the regenerative amplifier. This is because the maximum length of the pulse, measured in length units rather than time units, has to fit within the round-trip length of the regen. After testing of several regen candidates early in the NIF Project, the design of the regen was chosen for optimized output-energy stability. The physical length of the regen represents  $\sim 45$  ns, but after accounting for the rise and fall times of the Pockels cell used to switch the pulse out of the regen for injection into the next level of pre-amplification, the longest pulse it can handle varies from 32–35 ns, depending on individual beamline parameters; this is considerably longer (better) than the 20 ns originally specified for NIF.

Validation that pulses longer than 20 ns can be delivered is shown in Fig. 19 where a  $1\omega$  shot was taken for confirmation of non-closure of the 150  $\mu$ rad TSF4 pinhole for all 48 quads after a pinhole-size reconfiguration. All beams in all clusters participated in this demonstration, using 2 clusters at a time on 2 different shots. This image for B147 is typical with a high picket of 1.3 TW/beam followed by a long  $\sim 28$ -ns 150-GW flat pulse. The fact that the long flat pulse was not distorted was evidence that pinhole closure did not occur.

### ***II.H.1 Laser Pulse Shape***

Other than requiring the output pulse from NIF to be “shaped”, the FR&PC are silent about details of the pulse shape. From the early days of laser/target experiments that continued through Shiva, Nova, and the time of writing the NIF Laser Design and Cost Basis Document, a

general understanding developed between target and laser designers that exquisite pulse shaping would be required for meeting the ICF challenge.

The change in paradigm for design of the master oscillator, from using bulk optical components (used for all lasers from Janus to Nova) to a design born of fiber-optic telephonic technologies also introduced the capability for precise pulse-shape control never before possible. With these technologies, the NIF master oscillator is able to deliver a wide range of pulse shapes such as those shown in Fig. 20.

Pulse-shape control is provided by the AMC, described in “Description of the NIF Laser” (in this issue of *FS&T*), where 140 variable amplitude impulse generators are dedicated to each quad. With these spaced  $\sim 250$  ps apart, NIF can support shaping of pulses up to almost 35 ns. Current configuration of the variable amplitude impulse generators supports an initial rise time of  $\sim 100$  ps and a rise time of an internal section of the pulse of  $\sim 400$  ps. It would be possible to allow internal rise times as short as  $\sim 100$  ps with realizable (technology is available at a reasonable cost) modifications to the AMCs. In addition to pulse-shape control provided by the AMCs, the MOR can deliver short, approximately Gaussian shaped,  $\sim 88$ -ps impulses.

Pulse shape and timing is designed for the output of a quad; individual beams in the quad will have somewhat different pulse shapes due to variations in the power-dependent conversion efficiency of the different beamlines with the overall output from the quad meeting the desired shape. Each quad may be independently configured for timing and pulse shape. The MOR fiber system has also frequently demonstrated an “additive” feature that allows new pulse shapes, diagnostics, and pulse-shaping systems to be incorporated into NIF. Two recent examples of this flexibility are ARC pulse generation and preparations for Polar-direct-drive experiments.

The ability to make precise adjustments to the  $3\omega$  pulse shape was demonstrated in July 2007. Precise shaping and pulse-shape repeatability were both demonstrated as shown in Fig. 21 where the results for 28 shots are illustrated. Sixteen of these shots were taken to demonstrate repeatability, shown in the blue line of Fig. 21. The other 12 were both a test of repeatability and precise shaping compared to the first 16 shots. This test was completed using 1 beam diagnosed by the  $3\omega$  power sensors in the PDS (described in Section II.J). For the repeatability test, the beam was set up and fired 16 times for an identical pulse shape. For the shape-shifted test, that same beam was set up and shot for 12 times with a slightly different requested pulse shape. For the shape-shifted shots the second shock was specified to have 10% higher power, and the rise time of the third shock pulse was delayed compared to that for the first set by  $\sim 100$  ps.

## **II.I Pre-Pulse Intensity**

The NIF pre-pulse requirement is set for 96 beams. It is that “The laser intensity delivered to the target during the 20 ns interval prior to the arrival of the main laser pulse shall not exceed  $10^8$  W/cm<sup>2</sup>”. This requirement is intended to assure the integrity of the target at the time the main laser pulse arrives. Pre-pulse light would hit the windows of a typical target such as that shown in Fig. 22 and could cause preheat of the capsule inside.

At the time of NIF Project completion, Project personnel were faced with the still unsolvable issues related to the survival of any detector that could be placed at TCC for even the lowest-possible-energy NIF shot (known as a “regen shot”). In response, the strategy used for evaluation of the pre-pulse power combined low-power measurements at the input of the  $1\omega$  power amplifiers with calculations and measurements of high-power gain through those amplifiers and through the frequency-conversion crystals. This analysis was done on a per-beam basis. It was believed that only  $3\omega$  light could contribute to the pre-pulse power because  $1\omega$  light

would be directed away from the LEH by dispersion in the wedged final focusing lens. Measurements of the power injected from the ILS into the  $1\omega$  main amplifier yielded power levels of approximately 80 W of leakage from amplification before the 4-pass pre-amplifier and 60 W of amplifier spontaneous emission (ASE) that originated within the 4-pass pre-amplifier (for more information on the beamline design of NIF, see “Description of the NIF Laser”, also in this issue of *FS&T*). The measured gain for a  $1\omega$  main laser amplifier chain in its typical configuration was found to be at most 90,000, giving a  $1\omega$  output power of  $\sim 7$  MW (compared to a 1-beam limit for pre-pulse of 1.5 GW) and a  $3\omega$  converted power level of  $\sim 5$  mW. After taking into account focusing of all 96 beams from each hemisphere, the pre-pulse intensity at  $3\omega$  was estimated at less than  $40 \text{ W/cm}^2$ , very safe compared to the  $10^8 \text{ W/cm}^2$  specification.<sup>7</sup>

Again, at the time of Project completion, separate measurement of the ASE out of the  $1\omega$  main amplifier chain yielded a value of less than the prescribed power limit per beam of 1.5 GW. Although this is within the pre-pulse specification, the result was somewhat unsatisfying because the data was taken under conditions where the signal was only approximately a factor of 2 higher than the noise. Within the past year, the diagnostic for ASE from the main amplifiers has been improved, and this possible source of pre-pulse light continues to be monitored with results similar to those found in 2009.

After concluding (with various review committees) that the pre-pulse requirement had been met at the time of Project completion, NIF staff continued to intermittently monitor pre-pulse behavior on NIF and continued to consider mechanisms that could contribute to a pre-pulse at the target. Several mechanisms were considered:

- Light from the flashlamps that pump the large  $1\omega$  amplifiers could be scattered off the slabs and sent down the beampath at either  $1\omega$  ( $1.053\ \mu\text{m}$ ) or  $0.375\ \mu\text{m}$ .<sup>26</sup> (In addition to excellent reflectivity at  $1.053\ \mu\text{m}$ , the transport mirrors have a reflecting bandpass centered at  $0.375\ \mu\text{m}$  for use by the  $3\omega$  alignment beams that operate at this wavelength. The reflectivity of these mirrors is kept very low at  $0.351\ \mu\text{m}$  for protection of upstream optics in the event that stimulated Brillouin scattered light comes back from the target at very near the  $3\omega$  operating frequency of the laser).
- Off-normal excessive  $1\omega$  light from the ILS could be amplified by the  $1\omega$  main amplifiers and converted to higher-than-expected levels of  $3\omega$  light at the LEH. Three possible sources for this type of  $1\omega$  light have been identified:
  - Reflection from a misaligned lens in the regenerative pre-amplifier (One lens is situated such that, if misaligned, it could contribute to scattering when laser pulse lengths exceed  $\sim 18\ \text{ns}$ .)
  - Scattering from a damaged rod or Pockels cell in the regenerative pre-amplifier (Component damage can occur. The regen is run at  $1\ \text{Hz}$  for extended durations during each system shot cycle.)
  - An incorrect bias voltage in the modulator section of the MOR, possible as MOR components age, then allowing light leakage into the pre-amplifiers
- Residual  $1\omega$  light could be scattered by dirty debris shields or aging optics into the region of the LEH.<sup>27</sup>

Analysis has concluded that light from the flashlamps is not a pre-pulse hazard, but all of the other candidate sources of excessive light from the ILS and scattering from FOA optics have been identified as possible hazards and are now regularly monitored.

After it was recognized that unexpected light from the ILS could lead to pre-pulse levels above the specification, databases for past shots were interrogated to identify those shots where this type of off-normal operation may have occurred. As described in the following paragraphs, the performance of target experiments and laser performance prior to 2013 were evaluated for any unexpected behavior that could be correlated with a higher-than-specified pre-pulse.

Cryogenic gas-filled hohlraums have a 200-nm-thick, IR-reflecting aluminum layer on the outside of their 1- $\mu\text{m}$ -thick CH windows used to protect the interior of the target hohlraum from heating due to IR radiation from the target chamber wall. If a pre-pulse is present it would first be absorbed in this opaque aluminum layer. It was recognized in 2013<sup>28</sup> that the NIF VISAR (velocity interferometer system for any reflector) diagnostic,<sup>29</sup> with its 680-nm laser operating at a mW-power level could be used as a time-dependent monitor of the integrity of that aluminum layer in addition to serving its primary purpose as a diagnostic for observing shocks as they break through the capsule wall of mirrored “keyhole” shock-timing targets.<sup>30,31</sup> Specifically, the portion of the VISAR probe directed towards the upper pole of the partially transparent CH capsule is also coincidentally (and conveniently) retro-reflected off the pressure-bowed, concave surface of the top aluminized LEH window. In 2012, streak camera measurements of this reflected VISAR light channel showed a partial drop in reflectivity up to several nanoseconds before  $t = 0$ , as seen in Fig. 23, now attributed to the loss of Fresnel reflectivity as the Al layer was vaporized. No such early time reflectivity drop was seen in the 2 other VISAR channels that are aimed at the hohlraum equator and at 45 degrees between the equator and the pole.

Figure 24 shows that the time of first drop in reflectivity becomes progressively earlier as the upper-quad,  $3\omega$  pre-pulse intensity increases in the time frame between  $-5$  and  $-0.3$  ns. The  $3\omega$  pre-pulse of Fig. 24 was found from calculating the frequency conversion of the measured  $1\omega$

pre-pulse levels for all upper 96 beams. The fact that a drop is seen suggests that any pre-pulse light received before  $-3$  ns is sufficiently weak so as not to melt the aluminum. We also note that at a sufficiently low  $3\omega$  pre-pulse intensity ( $<3 \times 10^8$  W/cm<sup>2</sup>), the first drop in reflectivity is delayed until  $-0.3$  ns, a time that corresponds to the leading edge of the main laser pulse first rising above  $10^9$  W/cm<sup>2</sup>. A fit to the data gives a threshold  $3\omega$  damage fluence for the aluminum of  $0.7$  J/cm<sup>2</sup>, consistent with simple heat-capacity estimates. Unfortunately, VISAR data was not also available for the lower LEH where calculated  $3\omega$  pre-pulse levels reached above  $10^{12}$  W/cm<sup>2</sup> on some shots. There is also no unambiguous correlation between high pre-pulse levels and the performance (yield,  $T_{\text{ion}}$  and mix) of DT cryogenic implosions performed during the period in 2012 when pre-pulse was often high. While many of these implosions suffered from high mix, these results can also be interpreted as due to the extended drive-pulse lengths used for these shots.<sup>32</sup> It is noted in passing that for the regenerative pre-amplifier configuration at that time, these long drive pulses also created the highest ( $>10^{10}$  W/cm<sup>2</sup>) lower-quad pre-pulses as a by-product.

Each of the identified sources of off-normal,  $1\omega$  pre-pulse light has a recognizable diagnostic signature; within the past year a number of changes have been made to improve the pre-pulse diagnostics for signature recognition, and the occurrence of pre-pulse due to these sources has dropped significantly. By the end of the 2014 calendar year these changes will be complete. At that time pre-pulse due to light from the ILS is expected to occur only infrequently and it will be possible to correct the problem before the next shot is taken.

More detailed analysis of scattering of unconverted,  $1\omega$  light by the high-value optics within the FOAs also indicates that a small amount of this light can get to the LEH, but analysis (and measurements, now with an active sensor at TCC) indicates that this source is a very small

contributor to pre-pulse at the target. However, this study has shown that it is important to consider the pre-pulse signal as the total of both  $3\omega$  and  $1\omega$  sources of light.<sup>33</sup>

The possibility of residual  $1\omega$  light being scattered into the LEH by either aging FOA optics or by a set of dirty DDS (the last optics before the target and the ones that protect the high-value optics) has been studied using the  $1\omega$  CW alignment laser (see Section 5.4 of “Description of the NIF Laser” in this issue of *FS&T*) and an active target configuration at TCC, as shown in Fig. 25. The active target uses a CMOS 10-bit imaging sensor. Scattered-light data measured by this active target are shown together with a sketch of the active target in Fig. 26. The observation was made at the target plane (at 7.7 m) where the  $1\omega$  light is still on its way to focus because the focal length of the lens at  $1\omega$  is 8.1 m. The curve identified in Fig. 26 as “Idealized diffraction calculation” is the result of a physical optics calculation of the pattern of light from the  $1\omega$  footprint of the 96 beams of a hemisphere as they would be received at the target plane, assuming CPPs in their  $2\omega$  position and otherwise perfect optics. This curve represents the lower bound of the fraction of scattered light that one could expect to measure.

If enhanced scattering by a DDS that has collected debris from previous target explosions (that immediately follow the implosions) is not managed, the  $1\omega$  light reaching the LEH, when combined with other  $3\omega$  pre-pulse light, can contribute to exceeding the pre-pulse requirement. Calculations and the measured data given in Fig. 26 indicate that a set of dirty DDSs could contribute as much as  $0.2 \times 10^8 \text{ W/cm}^2$  to the pre-pulse signal. The DDS used for the data given in Fig. 26 was at a level that would have required its removal from NIF. The transmission of DDSs is monitored on a regular basis, and they are replaced when a combination of their scatter and solarization loss exceeds 4% of their original transmission. See more information on DDS

monitoring in Section 7.13 of “Description of the NIF Laser”, also in this issue of *FS&T*. Special attention is being given to the condition of any DDSs that are present for shots that might be particularly sensitive to the presence of pre-pulse light higher than the original requirement set for NIF.

With the improvement of pre-pulse diagnostics, the automated monitoring of pre-pulse behavior after each system shot, and the continual monitoring of disposable debris shield transmission, the  $1\omega$  pre-pulse situation has been significantly improved. It is only infrequently that the pre-pulse requirement is not met, and this only occurs after hardware damage has been sustained or occasionally when an experimental target campaign goes into a regime that has not previously been explored.

## **II.J Laser Spot Size**

The intent of the term “spot size” in the original FR&PC document was to describe the size of the focused beam of a single NIF beam after correction by the adaptive-optics loop and without a CPP in the beamline. In time, this became known as the “focal spot size”. (See Sections 6.3.8 and 6.3.9 of “Description of the NIF Laser”, also in this issue of *FS&T*, for a description of the adaptive optics loop and Hartmann sensor used in NIF.) Measurement of the focal spot size provides a measure of the beam quality being delivered by the laser, but in general it does not represent the size of the beams as they enter the target. The envelope dimensions (also often called beam size or spot size) of the beams as they enter the target LEH are almost completely determined by the characteristics of the CPP that is located in the FOA for each beam. The CPP is one element of the beam-smoothing capability discussed further in the next section. Before beams are directed toward the target, their profiles are tailored and “smoothed” to reduce the peak intensity of the light as they are focused in the LEH. Reducing the intensity

brings it into line with long-held projections for the highest intensity that would be acceptable at the LEH of between  $3 \times 10^{14}$  and  $1 \times 10^{15}$  W/cm<sup>2</sup>. (Ref. 34) Lowering the intensity is necessary for reducing the likelihood of Laser Plasma Interactions (backscatter) that can cause part of the laser light to be reflected rather than absorbed by the target. Continuous Phase Plates<sup>35</sup> are “user optics” specified by the experimenter from an inventory of available choices described in Section 7.1 of “A Description of the NIF Laser”, also in this issue of *FS&T*.

It was realized at the time the requirements were established for NIF that power and energy constraints at TCC would make it nearly impossible to directly measure focal spot size at TCC with the required precision. Instead, it was specified that beam-size measurements could be made at an equivalent target plane. In response, the focal spot size of B316 was measured in the NIF Precision Diagnostic System (PDS). A schematic view of the PDS is given in Fig. 27 and its details are described in Ref. 6. At the time when these PDS measurements were made, it housed a production prototype of the NIF FOA with optics that were identical to the optics then being received for use on the target chamber. The transport optics used to redirect a beam from Quad 31B to the PDS were also very similar in wavefront quality to those now in use in the switchyard and target bay.

Demonstration of the focal spot size of NIF was completed in PDS as part of NIF Project completion.<sup>7</sup> Because the specification for spot size is a beamline and not a full-system parameter it was logical for this parameter to be measured at that time. The functional requirement for the focal spot size for NIF specified that the output from a beamline deliver 500 TW full-NIF-equivalent (FNE) into an aperture of less than 600- $\mu$ m diameter. The measurement made in PDS (see Fig. 28 [a]), demonstrated 500 TW (FNE) enclosed within a diameter of 330  $\mu$ m ( $-79, +61 \mu$ m), well within the 600- $\mu$ m requirement, demonstrating that the focal spot

size for a NIF beamline has been met. A measurement of 530-TW enclosed power within a 600- $\mu\text{m}$  diameter was also completed, indicating that the power outside of the main spot was falling off rapidly. Taken together these 2 measurements indicate that the beam quality of NIF is far better than demonstrated by any other large aperture laser.

As seen in Fig. 28 (b) the inherent NIF focal spot size (without a CPP present) is only very weakly dependent on peak power within the required operating range. After introduction of a CPP into the beam, the focal spot size influences only the edge roll-off of the tailored beam that hits the target. Because the inherent focal spot size of NIF beams is very stable, the tailored beam profiles at the target are also stable enough to meet user requirements for beam delivery to complex targets.

Meeting the challenging spot-size requirement was made possible because many subsystem flowdown requirements were first met, including correction of large-scale ( $>8$  cm) phase imperfections of the optics by the adaptive optics loop and managing non-linear propagation effects along the full lengths of the beamlines:

- $\Delta B$  held to  $<1.8$  radians
- High-optical-quality specs met for all transmissive and reflective optics, thus reducing the generation of high-spatial-frequency optical noise on the beams
- Cone pinholes included in the spatial filters for safe high-power trimming of high-spatial-frequency optical noise
- “Air turbulence” in enclosed beamlines kept low

Even though, as expected, it has not been possible to directly measure the focal spot size of NIF beams during full-system shots, two techniques have been developed for measuring characteristics of the beamlines from which focal-spot-size information can be obtained. One

technique measures focal spot sizes in NIF during rod shots (when only the regenerative and 4-pass pre-amplifiers are firing) without a CPP present in the beams. The TAS is used as the diagnostic for these measurements. This technique has now measured all of the NIF beamlines. The blue bars of Fig. 29 present a histogram of the values of the diameters that encircled 65% of the incident energy for every beamline as calculated from the TAS images. The TAS measurements were taken with the adaptive optics loop, including the deformable mirror actuators and the Hartmann sensors, operating to minimize the rms gradient for each beamline. The diameters for the beams studied by TAS and given in Fig. 29 indicate that all were well within the focal-spot-size design specification for NIF beamlines. Error bars have been estimated for the TAS data of  $\pm 10\%$  after consideration of the impact of stray light, background noise subtraction, CCD bit depth, and algorithms for the encircling diameter.

Examination of Fig. 28 indicates that for the precision measurements made in PDS for B316 the diameter for an enclosed power of 65% of the total was  $\sim 173 \mu\text{m}$ . By comparison to Fig. 29, this would indicate that B316 is a somewhat below-average beam with respect to focal spot size. The 65% enclosed-energy diameter of B316 was measured as  $168 \mu\text{m}$  with the TAS, quite close to that found in the precision measurement in PDS. Figure 30 compares the image of the focal spot of B316 measured in PDS with that found for the TAS measurement. Characterization of the low-light regions of these two images is slightly different because the PDS camera has a larger dynamic range than the TAS camera (in PDS a Peltier-cooled 16-bit CCD, in TAS a 10-bit CCD).

The second technique uses information regularly collected by the Hartmann sensors during full-system shots. The deformable mirror that works in cooperation with the Hartmann sensor was designed to provide 16 waves of wavefront correction for each NIF beamline. Thus a

flowdown requirement for the Hartmann sensor was that it be able to control the mirror over this full range. This led to definitions for the lenslet spacing, the camera resolution, and the lenslet focal length. These three, together with pixel dimensions of cameras available at the time, led to adoption of a 77-lenslet Hartmann array. As described here, the Hartmann sensor is also being used as a low-resolution wavefront monitor. It measures the average spread of ray angles within its wavelength measurement band (~16 to 80 cm) compared to an ideal reference beam at  $1\omega$ . This angular spread gives a measure of the focal-spot-size contribution of spatial wavelengths within this band. Although it does not represent a full measure of the spot size, because Hartmann data is collected on every shot, for any power, it allows monitoring of the relative focal spot sizes during full-system shots, over time, and for changes in laser configuration. Hartmann data collected during the 4 years of operating NIF indicate that no significant changes in focal spot size have occurred.

## **II.K Beam Smoothness**

From its inception the design of NIF included providing spatial and temporal beam conditioning. Beam smoothing is used on every shot in NIF. Without beam smoothing, at its focus at TCC the NIF laser would produce a small, high contrast (100%), very high intensity profile. Beam smoothing is used to reduce the intensity of the spikes, lower the contrast (over some short-time interval), and shape the beam in a manner that meets target size and irradiance requirements.<sup>36,37</sup> The key components for beam smoothing by spectral dispersion (SSD) are distributed along the laser beamlines, as shown schematically in Fig. 31. As of the date of publication, the minimum bandwidth of the modulation requested by users or mandated by safe operation is typically 30 GHz of 3 GHz SBS failsafe modulation (to prevent the occurrence of

Stimulated Brillouin Scattering in the large  $1\omega$  and  $3\omega$  downstream optics) and 45 GHz of 17 GHz SSD modulation. The blazed Littrow grating in the 4-pass pre-amplifier has 1050 lines/mm with 95% efficiency in its  $-1$  order. Half of the beams in each quad have vertical polarization (P polarization from the viewpoint of a vertical hohlraum wall) and the other half of the beams have horizontal polarization (S polarization from the viewpoint of a hohlraum wall) facilitated with the addition of a half-wave plate as one of the final optics. A description of how the beam-smoothing components work together is given in Section 7.10 of “Description of the NIF Laser”, also in this issue of *FS&T*.<sup>38</sup>

## **II.L Beam Focusing and Pointing**

The Functional Requirements and Primary Criteria specifies flexibility in beam focusing and pointing. This capability allows NIF to shoot a wide variety of targets and their backlighters. For a standard hohlraum target there are at least two aim points, one for the top LEH and the other for the bottom LEH of the hohlraum, separated generally by  $\sim 1$  cm. For backlighter targets, a subset of the beams is directed to an offset foil or wire target that may be up to 40 mm from TCC. Light hitting the backlighters generates an x-ray source that is used to radiograph the main target.

Each NIF beam can be pointed  $\pm 5$  mm to its right or left (the x direction for the laser beam and  $\pm 30$  mm up and down the y direction). The actual pointing range in target coordinates depends on the individual beam due to the incident angle with respect to the target. The focal range for a NIF beam covers a span of  $\pm 37$  mm along the z direction of the beam. The focusing and pointing characteristics of each beam are well known and experiments are set up to stay within the overall range of all of the beams. In general this means that the center of the LEH of a specific target can be placed within  $\pm 5$  mm of TCC. It is sometimes important to offset a target

within this range to meet the magnification requirements for the backlighter/diagnostic combination desired for a given target.

## **II.M Recovery Time**

The requirement for recovery time has been interpreted by the NIF Project and its various review committees to call for a turnaround time between laser shots of less than 8 hours. During the time for formal execution of the tests for meeting the NIF Project Completion Criteria, 2 separate sets of 3 full 96-beam system shots were completed with all sets taking less than 8 hours between shots. During that campaign 111 beams were actually delivered to the target chamber. The shortest time between 2 shots in that series was 5 hours and 10 min.

In general the ability of the laser to respond to a request for a shot is not a limiting factor for setting the time between facility shots. The series of shots taken in June 2012 shown in Fig. 32 were not a deliberate attempt to meet any shot-time-separation goal, they were just completed in the regular course of doing business in NIF.

The time between shots, as established only by the laser, is considered as the time it takes for the laser to once again be able to meet its requirement for focal spot size after amplifier glass and other optical components have been heated by a previous shot. Following a shot, heating distortion of the optics increases the focal spot size at the focal plane. Figure 33 illustrates the impact on focal spot size of slab heating for the Beamlet laser.<sup>39</sup> Figure 34 illustrates the difference in focal spot size for NIF with and without the deformable mirror loop operating.

The length of time between laser shots is shortened first of all by cooling of the flashlamps and slabs using temperature-controlled, clean-dry air driven through the large set of pipes just above the amplifiers as shown in Fig. 35.

Further shortening of the time between laser shots is provided by operation of the deformable mirror loop that includes a set of actuators attached to the back of Laser Mirror 1 (LM1) as seen in Fig. 36, a Hartmann sensor located in the Output Sensor Package (OSP), and the Integrated Computer Control System. See “Description of the NIF Laser”, also in this issue of *FS&T* for the location of the LM1 actuators and the Output Sensor Package.

Tests on NIF have demonstrated that with cooling of both the slabs and the flashlamps, and with the NIF deformable mirror loop, NIF can conduct around-the-clock operation with a four-hour-shot period and no significant focal-spot-size degradation. Additionally, “burst” mode operation for shot periods as short as one-and-a-half hours is possible with minimal increase in focal spot size.<sup>40</sup>

## **II.N Laser Diagnostics**

The Functional Requirements and Primary Criteria describe the diagnostic capabilities required in NIF for verification that the laser has met its FR&PC performance requirements. It calls for the ability to measure the following:

- Laser pulse energy and power
- Laser pulse duration and dynamic range
- Laser beam power balance
- Simultaneity of arrival of pulses from individual beamlines at TCC with 10-ps accuracy
- Laser beam pointing accuracy with 10–20  $\mu\text{m}$  spatial resolution
- Laser pre-pulse intensity
- Laser pulse spot size

- Laser pulse smoothness
- Laser beam thermal recovery time

This requirement for optical diagnostics was met with the capabilities of the PDS, described earlier, and with the set of diagnostics that are in regular use to setup and operate the NIF laser. A top-level diagram of the diagnostics used for regular laser operations is shown in Fig. 37.

Cost and practicality considerations led to design of the regularly used diagnostics package shown in Fig. 37, where a combination of measurements and results of calculations are used to infer the performance at other locations not directly diagnosed. The PDS and the well-proven capabilities of the NIF propagation codes were used to validate that this package design could diagnose the necessary laser operational parameters for minimum capital cost.

The “in regular use” diagnostics are used to do the following:

- Measure energy
  - At  $1\omega$  at the input to the regenerative amplifier (1 per quad, measures quad sum)
  - At  $1\omega$  at the output of each Pre-amplifier Module (1 per quad, measures quad sum)
  - At  $1\omega$  at the output of the main laser (4 per quad)
  - At  $3\omega$  at the output of the FOA (all beams, 4 per quad)
- Measure power
  - At  $1\omega$  at the input to the regenerative amplifier (1 per quad, measures quad sum)
  - At  $1\omega$  at the output of each Pre-amplifier Module (1 per quad, measures quad sum)
  - At  $1\omega$  at the output of the main laser (2 per quad)

- At  $3\omega$  at the output of the FOA (1 per quad except for Q34T, Q31B, and Q36B. On these quads each beam had a power sensor. B34 was used in the Single-Bundle PCC.)
- Measure near-field images
  - At  $1\omega$  at the output of each Pre-amplifier Module (PAM)
  - At  $1\omega$  at the output of the main laser (4 per quad)
- Measure far-field images
  - At  $1\omega$  at the ISP
- Wavefront
  - At  $1\omega$  at the output of the main laser (4 per quad—Hartman sensor located in OSP)
- Wavelength and bandwidth at the output of the master oscillator (1 set for each of the inner cones and 1 set for the outer cones)

As described earlier, PDS diagnostics were used for the focal-spot-size measurement.

The ability of the pulse-synchronization measurement to resolve  $\sim 10$ -ps timing jitter in the ability to trigger a regen impulse shot was also illustrated earlier in Fig. 9, where the response of the target to laser impulses was recorded by the pulse synchronization measurement diagnostic system.

After each system shot, data from each of these diagnostics is processed by the Laser Performance Operation Model (LPOM) analysis package. The appropriate calibrations are applied to the raw data and resultant laser energies, powers, wavefronts, and bandwidths are recorded and compared to the values predicted prior to the system shot. The history of predicted and realized performance has been very good.

### ***II.N.1 Error Analysis of NIF Energetics***

This section discusses the error bars associated with the Drive Diagnostics (DrD) package that monitors the output of the NIF beamlines. The location for the calorimeter for measuring the output energy of each beamline can be seen in Fig. 38. Power measurements are made for at least 1 beam in each quad using fiber-fed vacuum photodiodes (60-ps rise time, 90-ps fall time Hamamatsu R1328U-52) and near-field profile measurements are available for a few beams using a CCD camera package that can be moved from beamline to beamline. Section 7.12 Drive Diagnostics in “The Description of the NIF Laser” in this issue of *FS&T* provides more detail on the geometry of pickoff and the design of the DrD optics and hardware. Figure 38 also includes a CAD perspective view of the relationship of the DrD package with respect to the FOA and the beam converging toward the target.

Table II includes an analysis of the error bars associated with calorimetric energy measurements in an environment where target debris from previous shots is included as a possible generator of optical noise. Each of the NIF calorimeters is a tertiary standard calibrated against an LLNL-owned secondary standard, which was calibrated by comparison to a NIST primary standard in the LLNL Calibration Laboratory. The  $\sim 0.1\%$  beam sample for the DrD is provided by diffraction from the shallow ( $\sim 15$  nm) grating on the uncoated side of the Grating Debris Shield (GDS) located in the converging beam beyond the focusing lens. Before being installed, the sample fraction provided by each GDS was measured in an offline calibration laboratory at LLNL, using the Diffractive Optics Full-Aperture System Test (or DOFAST). The dominant source of forward-going stray light into the DrD is scattering of the main beam by target debris deposited on the DDS optic during previous shots. Light backscattered from the target at near the  $3\omega$  wavelength (stimulated Brillouin scattering) can get into the DrD by first

being partially reflected by one of the Integrated Optics Module (IOM) optics, for example, by the doubler crystal. Any light that is reflected by the doubler is once again going “forward” and some of it can then be diffracted into the calorimeter, following the same path as that of light from the main beam that was diffracted toward the sensor  $\sim 54$  ns earlier. For the error analysis, noise from this source was quantified by assuming a value for the maximum backscatter energy expected, the expected backscatter cone angle, and the reflectivity of various IOM optics at  $3\omega$ . The result given in Table II was validated by taking back-to-back identical shots with and without the presence of a target.

Table II includes a source of error that is the result of the non-common path of light through the DDS. At the DDS, the footprint of the diffracted light going to the DrD is smaller than the footprint of the main beam going toward the target. Two-thirds of the diffracted beam has a common path with the main beam, and one-third of the diffracted light goes through a region of the DDS that is not illuminated by the main beam. Two effects that act in opposition are experienced in this region. Here, the transmission of the DDS will be higher because it does not experience the solarization induced by the main beam, and the transmission will be lower because it does not experience laser cleaning of target debris that is collected approximately uniformly across the DDS. Circa 2014, DDS transmission could be modeled on the basis of shots it had previously experienced. This model was calibrated by monitoring the DDS transmission every few shots using the  $0.375\text{-}\mu\text{m}$  alignment laser as a light source and the TAS alignment sensor as an energy diagnostic. The insertion and removal capability of the Automatic Disposable Debris Shield system provides the ability to measure the DDS transmission as the ratio energy detected by the DrD sensors with and without the DDS inserted in the beam. A

model included in LPOM keeps track of the solarization and debris deposition for the DDS on a shot-by-shot basis.

More information on the topics discussed in this section can be found in other locations in this issue of *FS&T*. Section II.F of this article, “Beamlet Positioning, Pointing Accuracy” discusses the TAS sensor. Sections in “Description of the NIF Laser” discuss the following topics:

- Section 4.0—Beam Propagation Codes and the Laser Performance Operations Model—for LPOM
- Section 7.13—Automated Disposable Debris Shield System—for the ADDS system and more details on the LPOM model of solarization and debris deposition
- Section 9.0—NIF Laser Alignment—for the 0.375 light source and the TAS sensor

After the various sources of error summarized in Table II have been taken into account, the  $1\sigma$  percent error expected for NIF energy measurements is  $\pm 3\%$ .

### **III. SUMMARY**

This article illustrates that NIF has met and now meets all of its original requirements. In general its performance is now better or much better than originally requested. During 2013, customer surveys were sent out to Shot RIs for 174 target shots asking about their experience with NIF. This survey covered the entire facility, including their experiences with targets and target diagnostics, not with only the laser. Ninety-four percent reported total satisfaction. The most common introductory comment given as shot reviews were discussed was “The laser performed as requested!”

TABLE I. Summary of the Functional Requirements and Primary Criteria (FR&PC) for the NIF Laser System (measurements in green indicate meeting the FR&PC; measurements in light green are for criteria established specifically for Project Completion) (online the table is given in color).

FR&PC Rev 1.8	Level 1 Primary Criteria	Project Completeion Criteria		Full-NIF FR&PCs
		Perf Bundle	96 Beams	
2.1.1	Laser Pulse Energy	≥ 75 kJ	≥ 500 kJ	≥ 1.8 MJ
2.1.2	Laser Pulse Peak Power	≥ 21 TW	≥ 200 TW	≥ 500 TW
2.1.3	Laser Pulse Wavelength	0.35 μm	0.35 μm	0.35 μm
2.1.4	Beamlet Power Balance	For Rev 3.1	For Rev 3.1	RMS quad deviation averaged over 2 ns, from Rev X point design spec
2.1.5	Beamlet Positioning Accuracy	≤100 μm rms	≤100 μm rms	≤50 μm rms
2.1.12	Direct-Drive Requirements	Not precluded	Not precluded	Shall not to be precluded
3.3	Laser Safety	Always	Always	Comply with ANSI Z136.1
7.2	Recovery Time	≤ 8 h	≤ 8 h	≤ 8 h between full system shots

FR&PC Rev 1.8	Level 2 Functional Reqmts	Project Completeion Criteria		Full-NIF FR&PCs
		Perf Bundle	96 Beams	
2.1.6	Laser Pulse Duration	Up to 20 ns	Up to 20 ns	Up to 20 ns
2.1.7	Laser Pulse Dynamic Range	≥ 50:1	≥ 25:1	≥ 50:1
2.1.8	Capsule Irrad Symmetry	By design	By design	2 cones/hemisphere, ea w ≥ 8 beams
2.1.9	Prepulse Power	<4-10 <sup>8</sup> W/cm <sup>2</sup>	<10 <sup>8</sup> W/cm <sup>2</sup>	< 10 <sup>8</sup> W/cm <sup>2</sup> per hemispere
2.1.10	Laser Pulse Spot Size	≤ 600 μm	≤ 600 μm	Design energy within ≤ 600 μm
2.1.11	Beam Smoothness	Spatial/Temp	Spatial/Temp	Shall have ability to do spatial and temporal beam conditioning
2.1.13	Beam Focussing & Pointing	By design	By design	Should have flexibility for users
2.2.8	Diagnostic Capability	By design	By design	See chart in Laser Diagnostics Sec

TABLE II. Error breakdown for the Drive Diagnostic (DrD) energy measurement for a single 3 $\omega$  laser beam.

Contributor	Sub-Contributor	Error (% 1 $\sigma$ )			
		Current Estimate		Design Budget [##]	
		Rel.	Abs.	Rel.	Abs.
Calorimeter	DrD Stability	0.3		1.0	
	Rel. Calibration Accuracy (relative)	0.5			
	Abs. Calibration Accuracy (NIST-NIF Ref.)		0.7		4.0
Beam sample from GDS	Abs. Calibration Accuracy (DOFAST*)		2.5		
	Rel. Calibration Accuracy (DOFAST*)	0.6		1.0	
	Coupling to Beam Size and Shape	0.3			
	Stability	1.0		2.0	
Correction for stray light	Forward-Going Beam	0.4		0.5	
	Target back scatter	0.6		1.2	
Correction for non-common path thru DDS	Solarization and Debris	<0.1		0.2	
	Nonlinear Transmission	<0.2			
Sub-Total		1.5	2.6	2.8	4.0
Total		3.0		4.9	

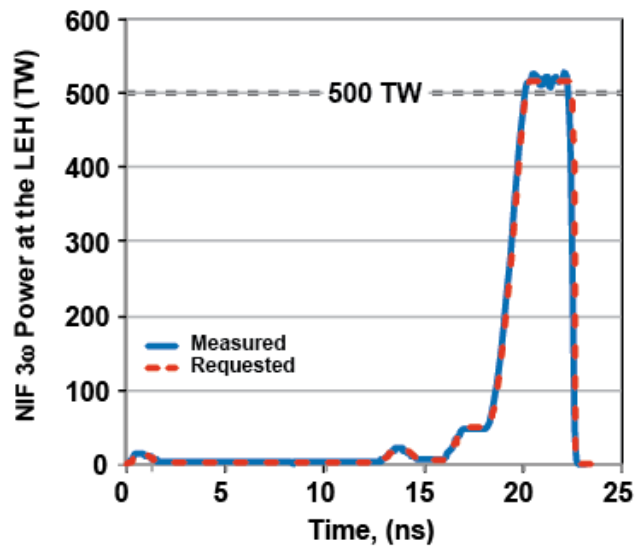


Fig. 1. Pulse shape for shot N120705-002-999, July 5, 2012.

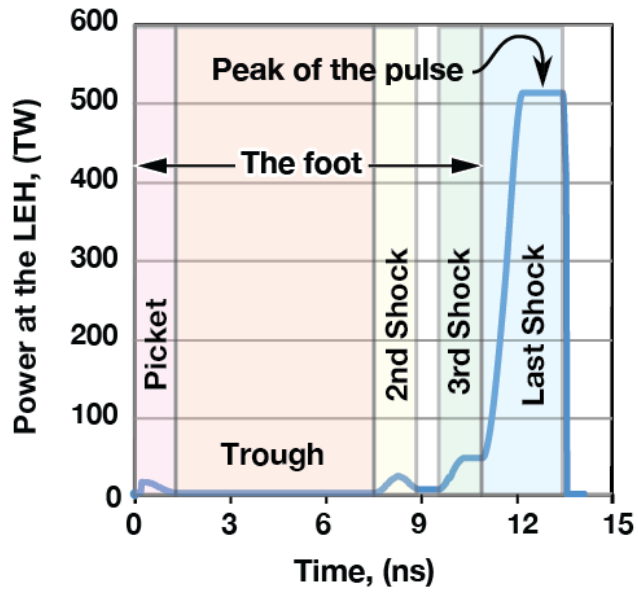


Fig. 2. Terminology typically used to describe ICF-like laser pulses.

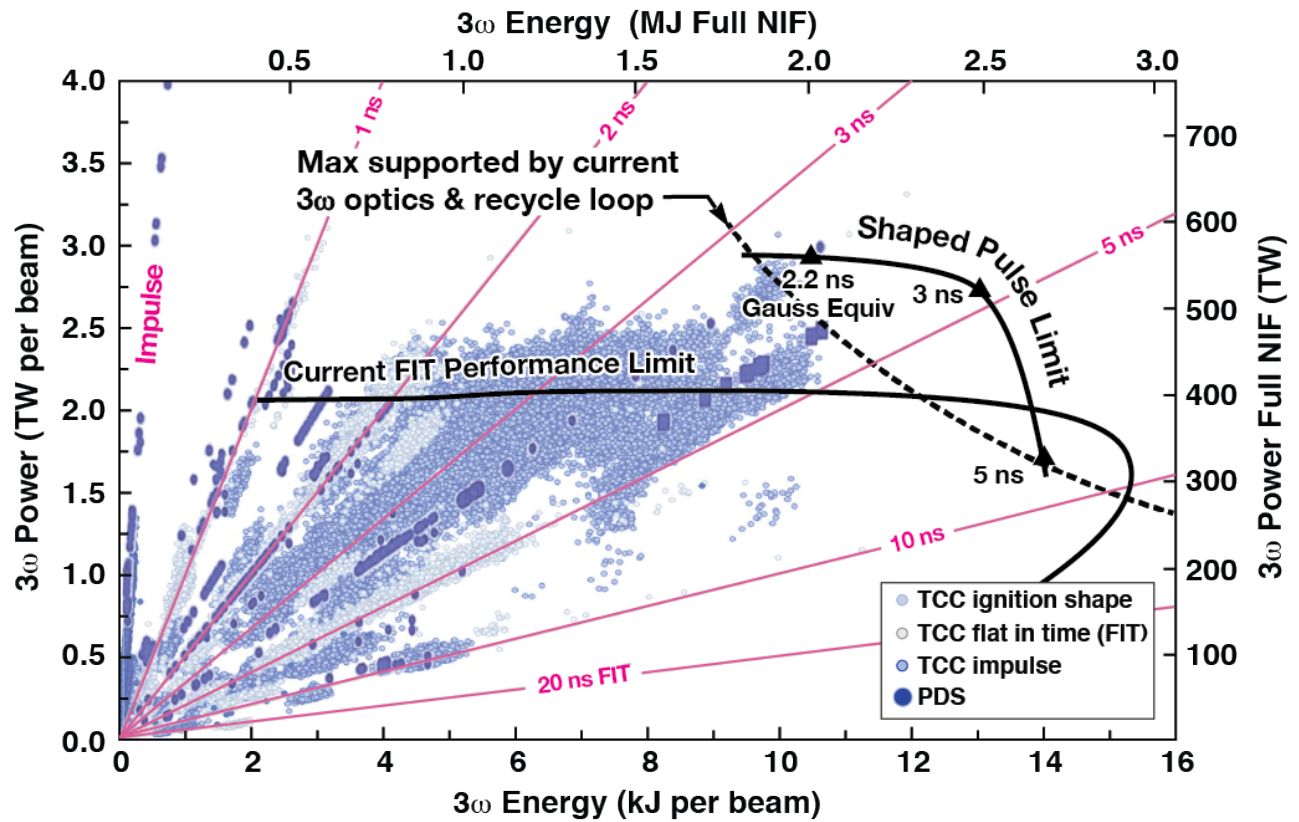


Fig. 3. Sustainable operational energy and power limits overlaid on a plot of measurements of pulse energy and corresponding power for shots up until July 2012. Flat in time (FIT) pulse performance and performance with higher contrast “shaped” pulses are summarized.

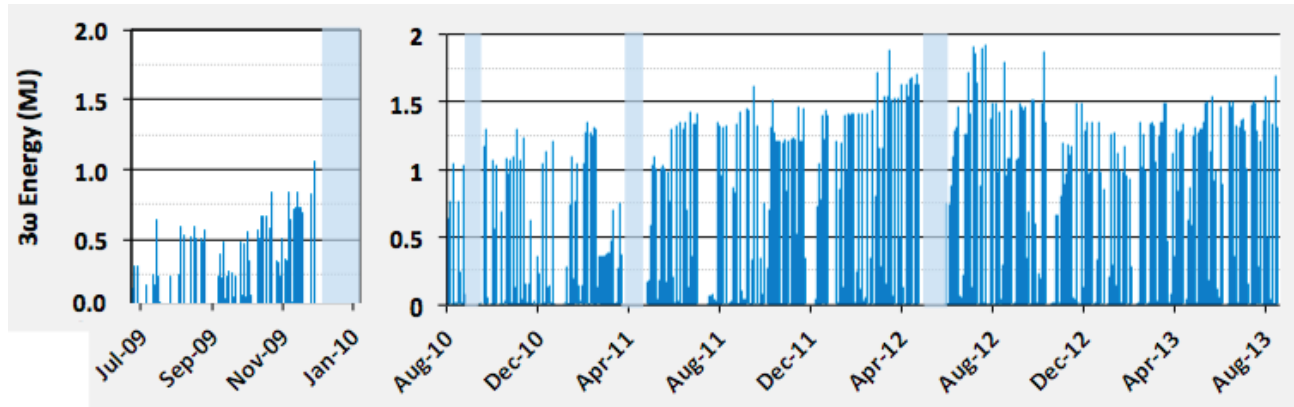


Fig. 4. Time history of  $3\omega$  shots taken at NIF between 2009 and 2013. Gray areas indicate time periods for completion of routine maintenance and upgrade tasks.

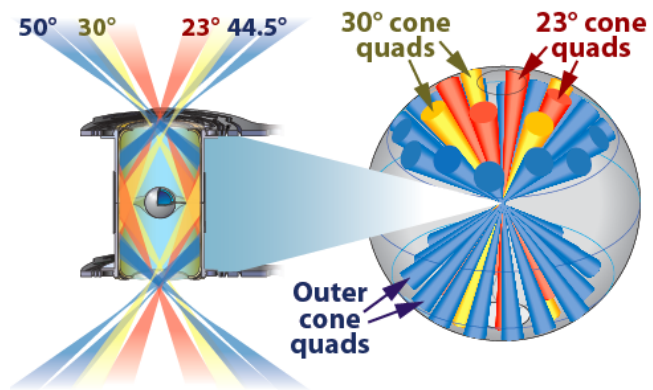


Fig. 5. Cone and beam symmetry architecture of the NIF. Note that light from the lasers enters the hohlraum through Laser Entrance Holes (LEHs) in the top and bottom of the cylindrical hohlraum target.

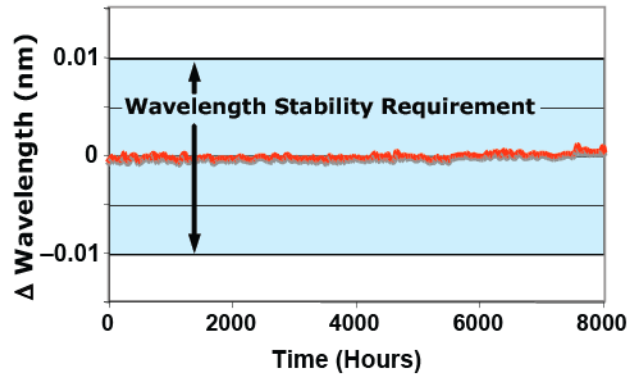


Fig. 6. A segment of the outer-cone, wavelength-stability measurement that extended over 11,000 hours during 2005 and 2006.<sup>40</sup>

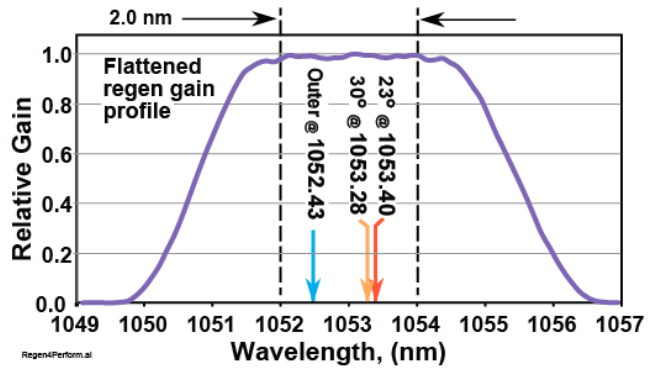


Fig. 7. Flattened gain profile and tuning range of the regenerative amplifiers in NIF. Specific wavelengths shown are for operation on July 25, 2012.

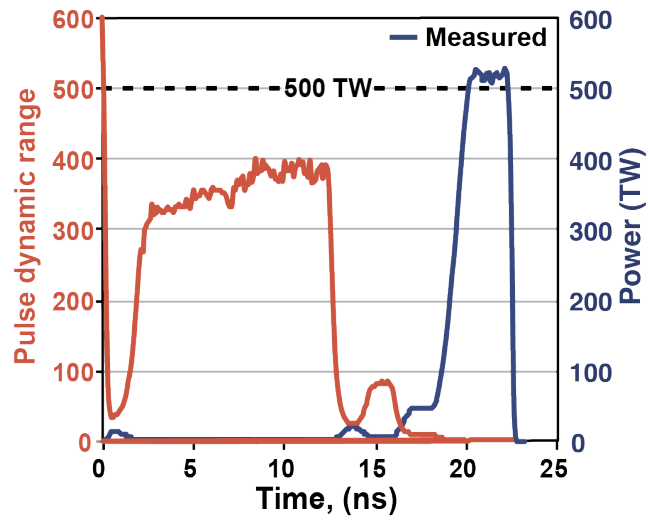


Fig. 8. The pulse dynamic range, given by the peak power in a pulse divided by the power at every instant in time for that pulse, for a NIF shot taken on July 5, 2012.

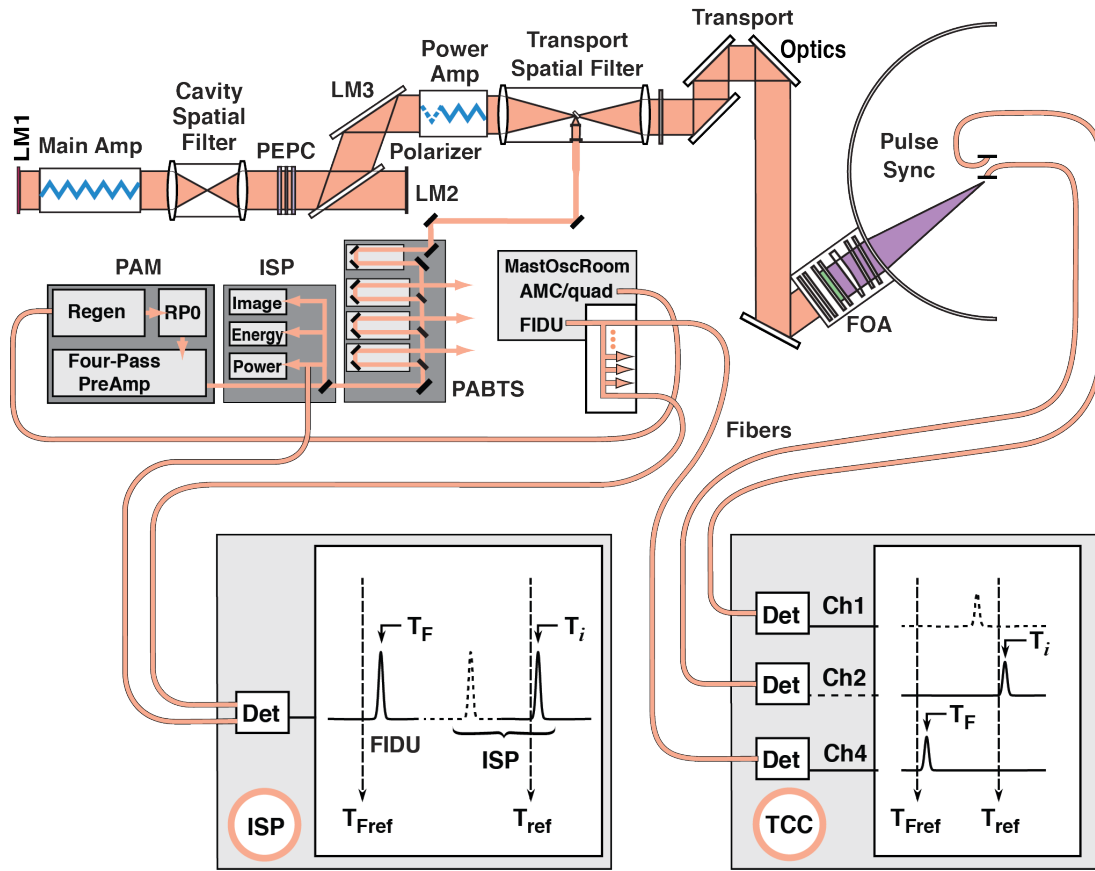


Fig. 9. Locations along a NIF beamline for measurement of the timing error of that beamline.

The schematic drawings in the top portion of the figure identify the source locations of the measured optical signals. The lower part of the figure provides views of the fast scope traces as they record those signals. The scope traces indicated here are for tests of a lower hemisphere beam. The dotted traces illustrate where the signals would appear for a corresponding top hemisphere beam. Only one beam at a time is evaluated.

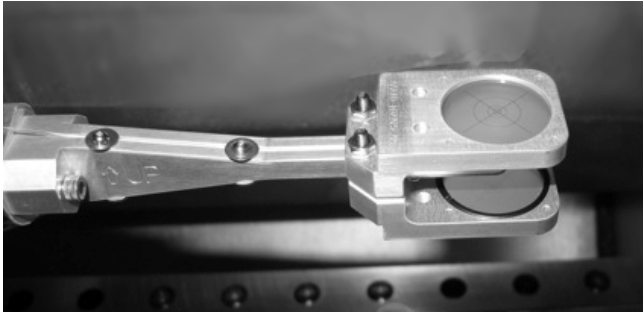


Fig. 10. Photo of the “pulse sync” synchronization target with scatter plates that couple light into fibers located between the two plates.

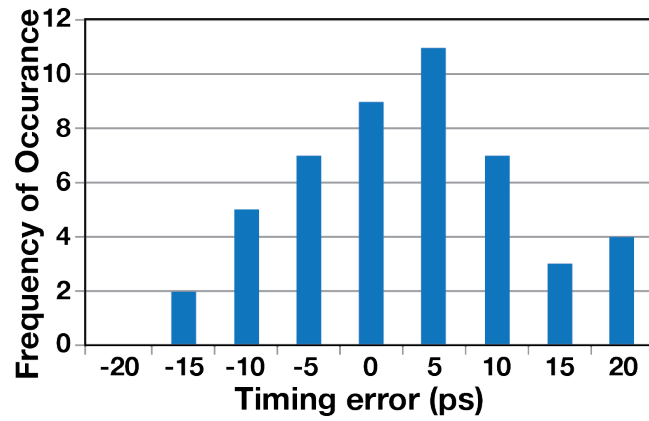


Fig. 11. Measurement uncertainty of the pulse synchronization system for a series of 274 measurements taken over a 2-day period in April 2012. The average uncertainty for the pulse synchronization system is  $\sim 10$  ps.

$$\text{Power Balance} = \sqrt{\frac{\sum_{i=1}^n \left( \frac{P_i^{sm} - \bar{P}_{cone_i}^{sm}}{\bar{P}_{cone_i}^{sm}} \right)^2}{n}}$$

Fig. 12. Definition of power balance for a NIF shot.

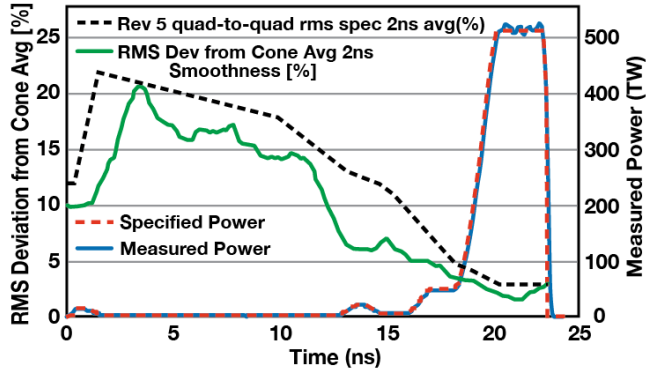


Fig. 13. Power-balance parameters of NIF for the full system shot taken on July 5, 2012, verifying that the power-balance requirement for NIF has been met.

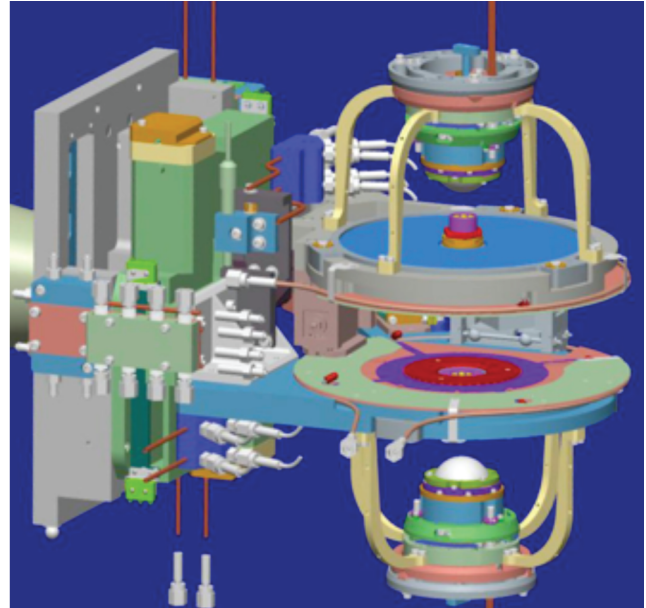
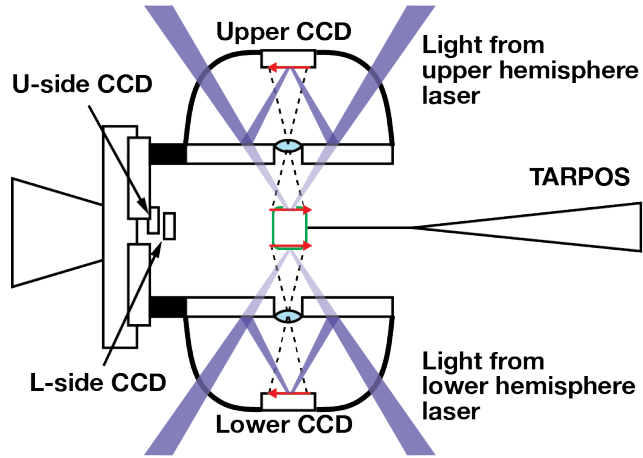


Fig. 14. The Target Alignment Sensor: (a) optical configuration of TAS surrounding a target held by the target positioner (TARPOS) (b) CAD view.

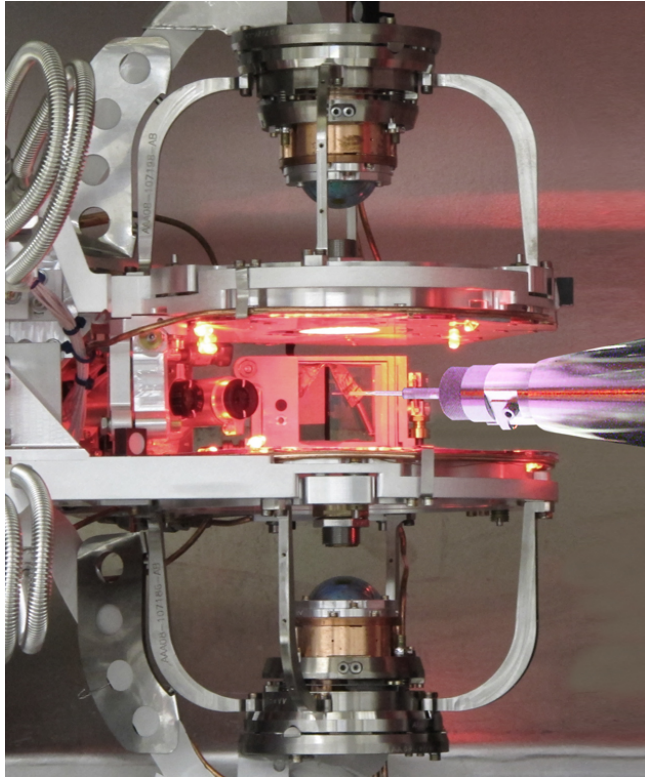


Fig. 15. Photograph of the TAS configuration with TARPOS holding a flat silicon-wafer target.

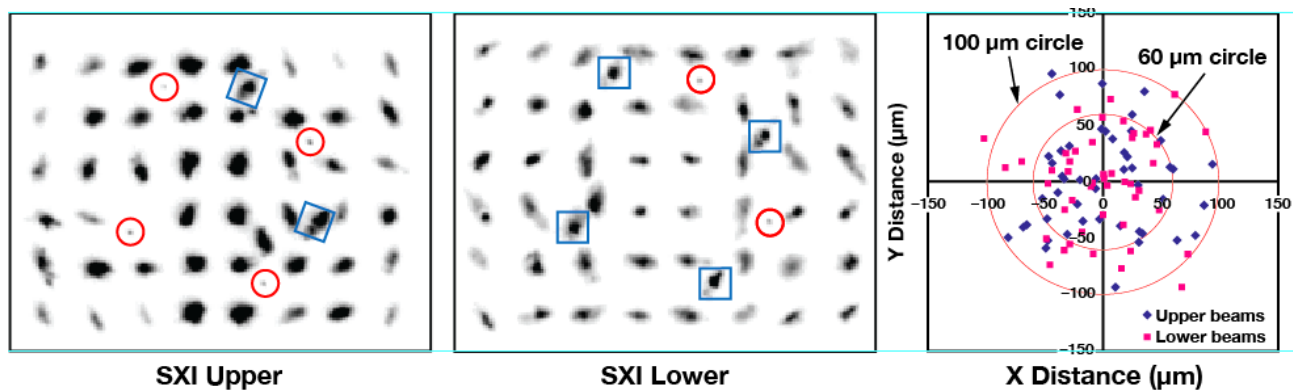
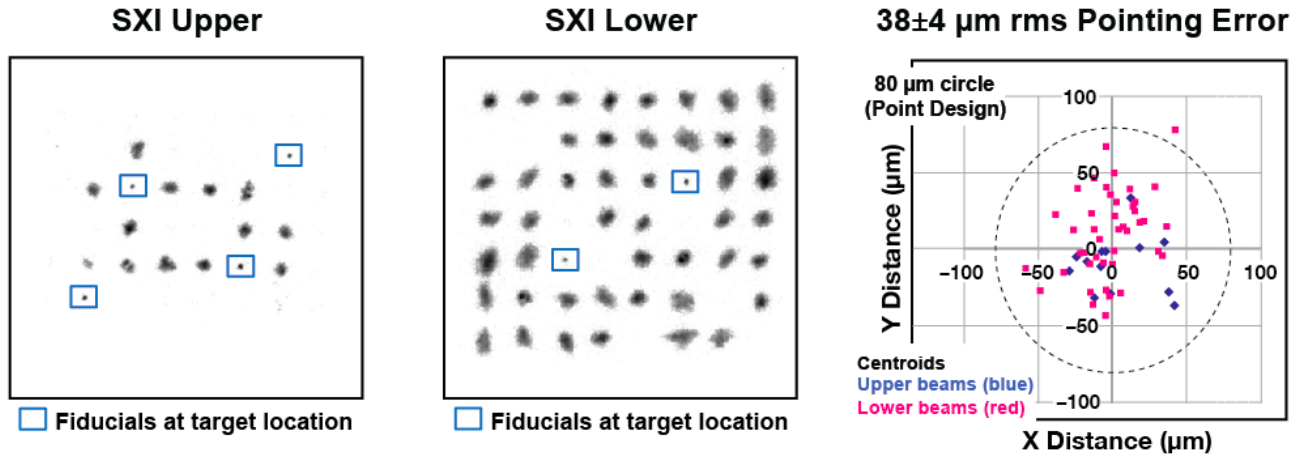


Fig. 16. X-ray images taken to verify that the Project Completion Criteria for target and beam-to-target alignment had been met for NIF: (a) image for the top hemisphere, (b) image for the bottom hemisphere, (c) beam positioning relative to the target as measured for Project Completion, giving an accuracy of  $<64 \pm 4 \mu\text{m rms}$ . The 100- $\mu\text{m rms}$  requirement is shown by the circle overlaid on the plot.



**X-ray images of focal spots, 700 microns between focal spots on new TAS camera**

**Shot N110427-002-999**

Fig. 17. Data summary for meeting the NIF Functional Requirements & Primary Criteria beam pointing requirement of <math><50 \mu\text{m}</math> rms on target. Pointing error for this shot was  $38 \pm 4 \mu\text{m}</math> rms, better than the requirement of <math><50 \mu\text{m}</math> rms originally specified in the Functional Requirements & Primary Criteria.$

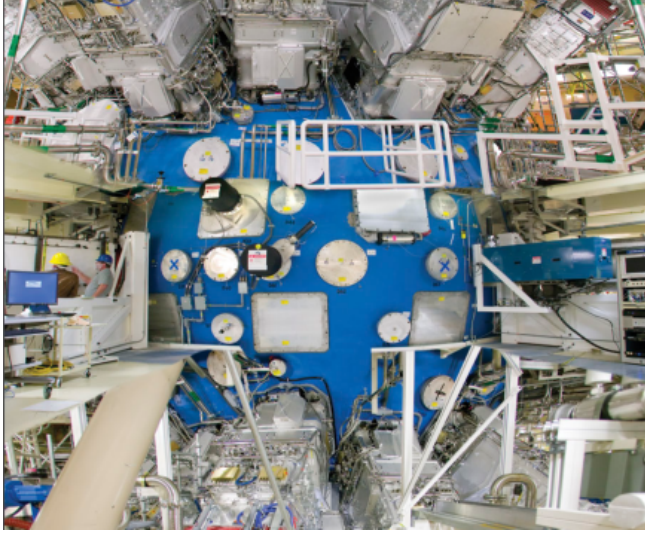


Fig. 18. Near-equator ports for Direct Drive final optics are seen here in both the upper and lower hemispheres of the 10-m-diameter NIF target chamber.

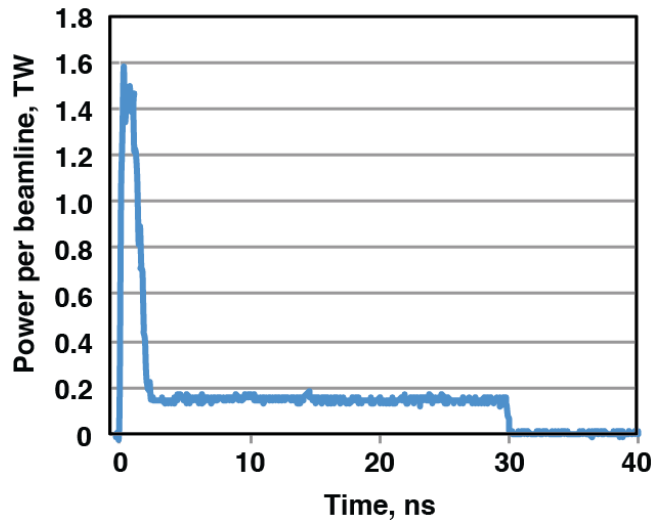


Fig. 19. The long pulse used in shot N120817-002-999 for the purpose of confirming that pinholes remained open for the entire 30-ns pulse length.

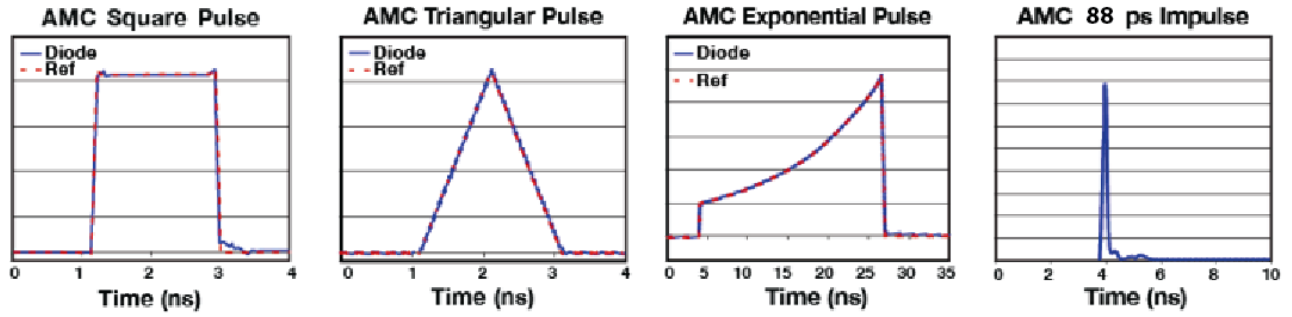


Fig. 20. Illustration of the broad range of pulse shapes that can be generated by a NIF  $1\omega$  master oscillator: (a) square pulse, (b) triangular pulse, (c) exponential pulse, (d) 88-ps impulse.

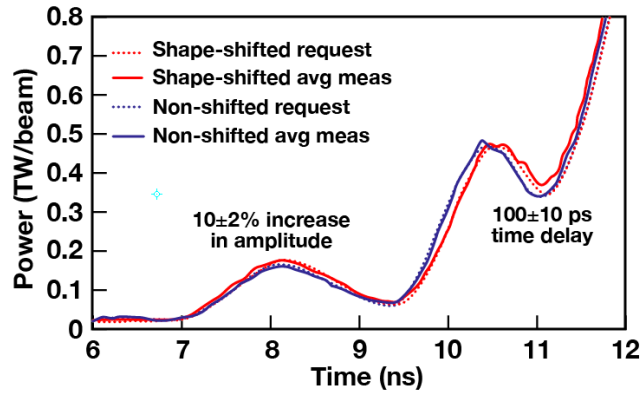


Fig. 21. Ability of NIF to deliver precision pulse-shape control and repeatability (average pulse shapes for 12 shots shifted, 16 shots unshifted).

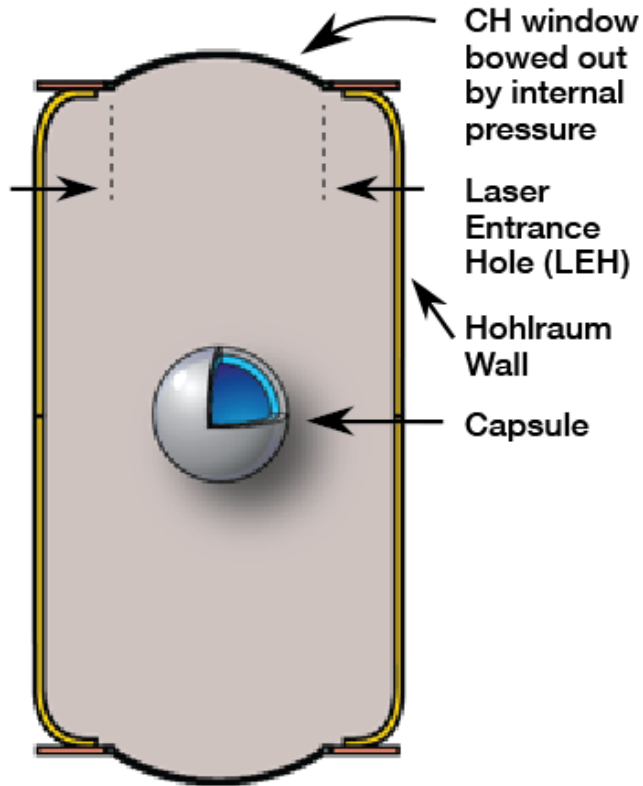


Fig. 22. Cross section of an ICF gas-filled target before the main laser pulse arrives, showing the hohlraum wall, capsule, LEH, and CH windows that are bowed out by the internal pressure in the hohlraum.

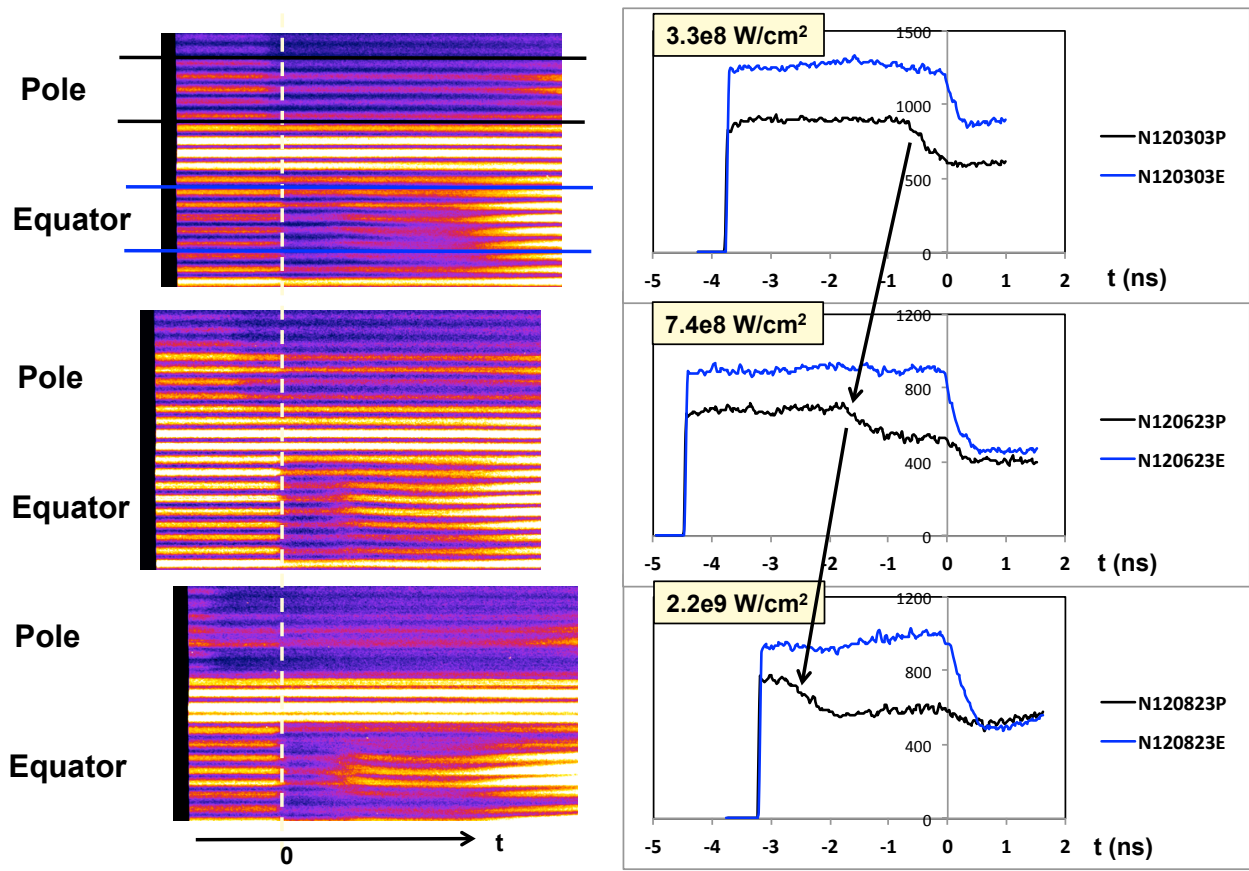


Fig. 23. VISAR streaks reflected off the top pole and equator of the capsule and their corresponding intensity lineouts for pole (black) and equator (blue) (online in color) for 3 shots ordered by increasing  $3\omega$  pre-pulse. Arrows point to the first reflectivity drop on the pole channel attributed to pre-pulse. Second reflectivity drop at  $t = 0 \text{ ns}$  is attributed to first x-rays from the main pulse melting the surface of the capsule.

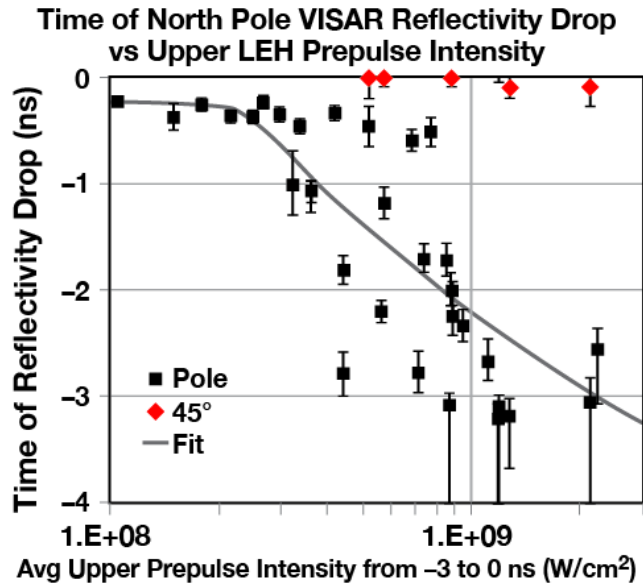


Fig. 24. Time of first VISAR reflectivity drop vs  $3\omega$  average pre-pulse intensity from  $-3$  to  $-0.3$  ns calculated as incident on the upper LEH window. Black is for the VISAR pole measurement; red (in color in the online version) is for the  $45^\circ$  measurement. Black curve is fit assuming reflectivity drop occurs at a given incident accumulated fluence, with best fit shown at  $0.7 \text{ J/cm}^2$ .

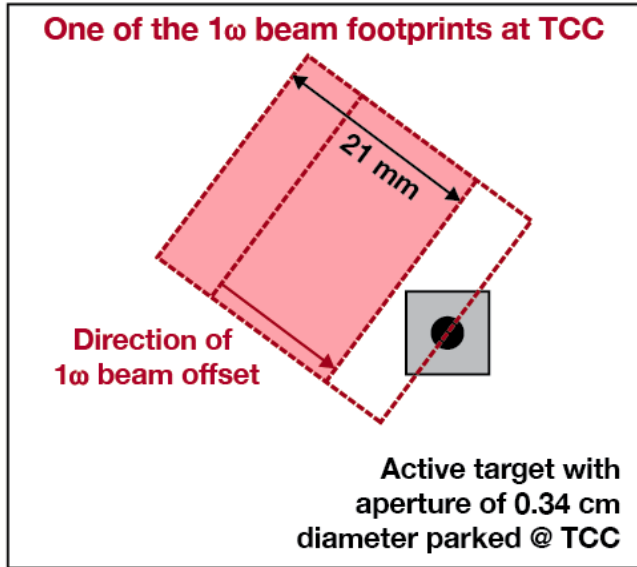


Fig. 25. A sketch of the configuration at target chamber center (TCC) used to measure the fraction of  $1\omega$  light that could be scattered into the area of a laser entrance hole (LEH) by  $3\omega$  focusing optics or dirt on the Disposable Debris Shields.

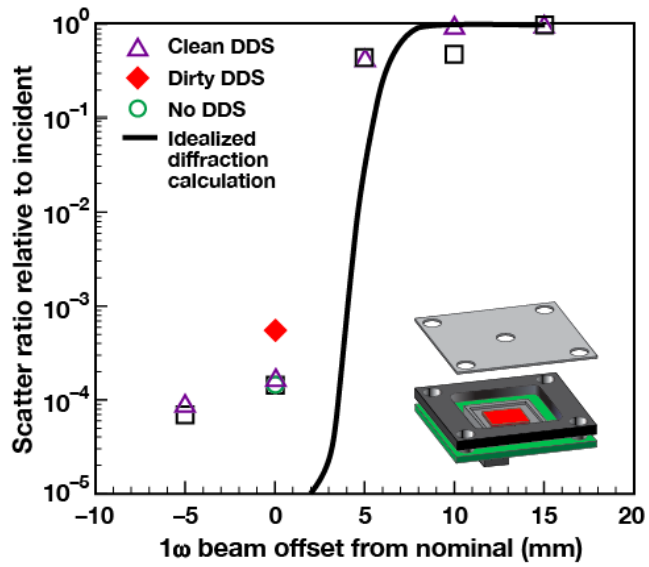


Fig. 26. Measurement of the relative amount of light hitting an active target with area similar to that for an LEH as a function of the distance of aim point of the  $1\omega$  light to the center of the active target (expressed as equivalent for 96 beams with the same scatter fraction of  $1\omega$  light).

Error bars for this data are estimated at  $\pm 20\%$ .

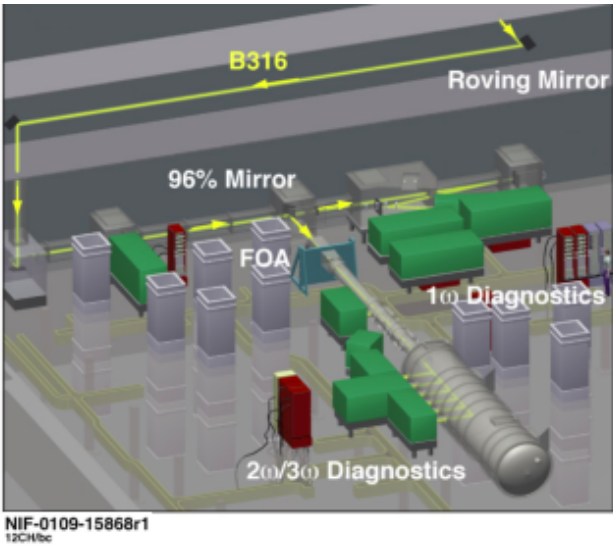


Fig. 27. Layout of the Precision Diagnostic System (PDS) used for verification of the design and performance of the NIF laser beamlines. In PDS, the beam energy and power were sent to an equivalent target plane and then allowed to continue into an evacuated tank. A small fraction of the beam power was then reflected by a large, uncoated, concave spherical mirror and directed to diagnostic tables where a suite of well-characterized, multi-wavelength diagnostics could accurately measure beamline performance.

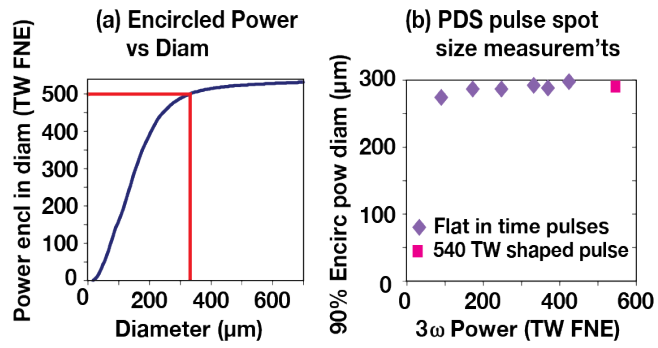


Fig. 28. The 500 TW “Full-NIF-Equivalent” (FNE) spot size of a NIF beam as measured in PDS:

(a) power encircled as a function of diameter, (b) focal spot size of a NIF beam as a function of the  $3\omega$  (FNE) power in that beam.

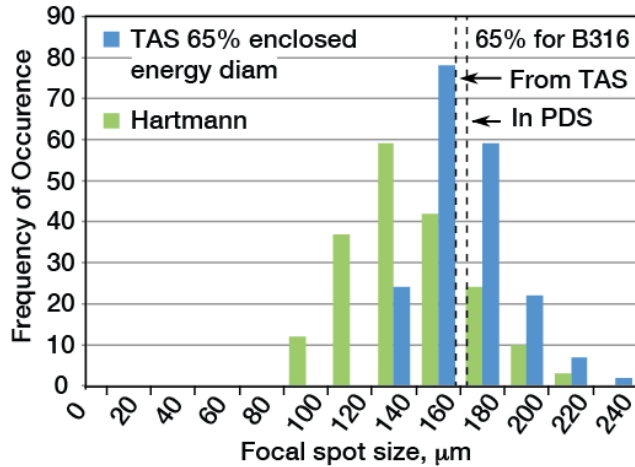


Fig. 29. (Online version in color) Blue bars are a histogram of the focal-spot-size distribution for 65% energy enclosed diameter for all of the beamlines in NIF, as measured with the Target Alignment Sensor (TAS) for rod shots. The two dashed lines are for B316, as measured in PDS and as measured with the TAS. Green bars are a histogram of the (Hartmann rms-gradient measurements)  $\times 2 \times$  (the wavelength,  $1.053 \mu\text{m}$ )  $\times$  (the focal length of the final focus lens). The green bars represent the low-spatial-frequency content of the focal spot and are not intended to be directly compared to the TAS measurements.

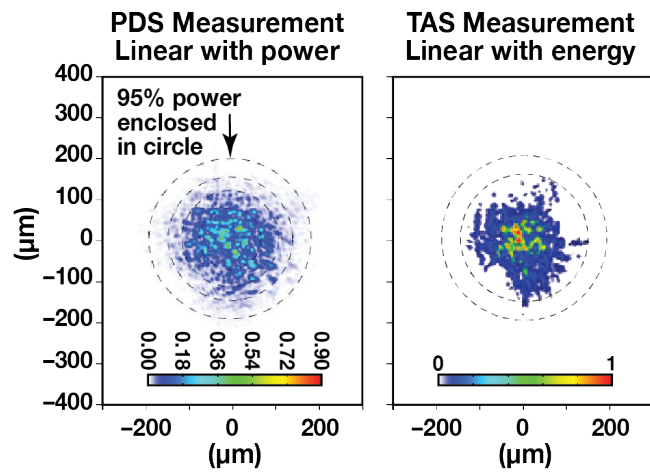


Fig. 30. Comparison of measurement of the focal spot size of B316 using two very different techniques: (a) the far-field image of a focused NIF beamline in the Precision Diagnostics System (PDS) as described for Fig. 27. (b) in NIF, for a rod shot using the Target Alignment Sensor (TAS).

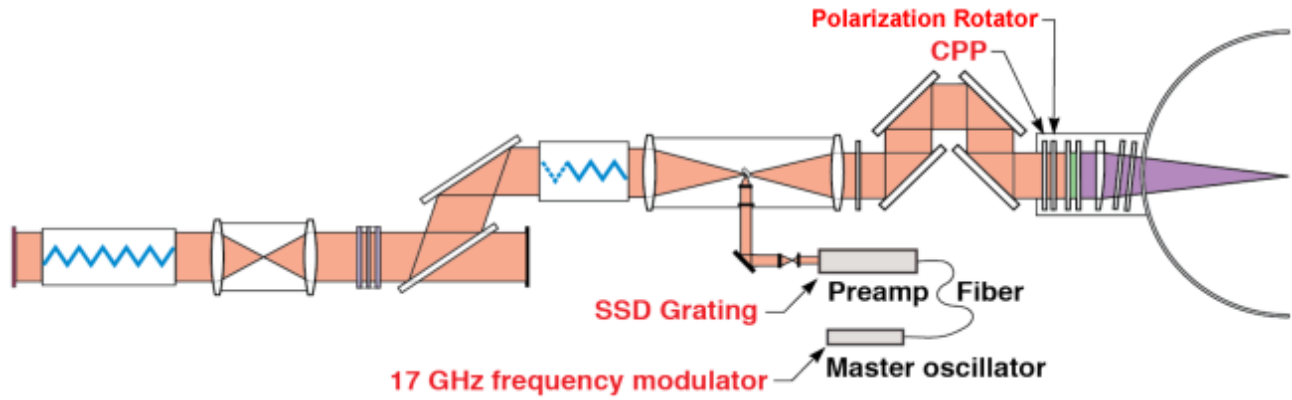


Fig. 31. Beam-smoothing components for NIF are distributed along the beamlines; the smoothing by spectral dispersion (SSD) modulators are in the Master Oscillator Room (MOR); a grating that adds angular dispersion as a function of the modulation resides in the four-pass preamplifier section; and a continuous phase plate (CPP) and polarization rotator are housed in the Final Optics Assembly (FOA), just before entrance into the target chamber.

**Time between full-system shots  
for the early June 2012 shot schedule**

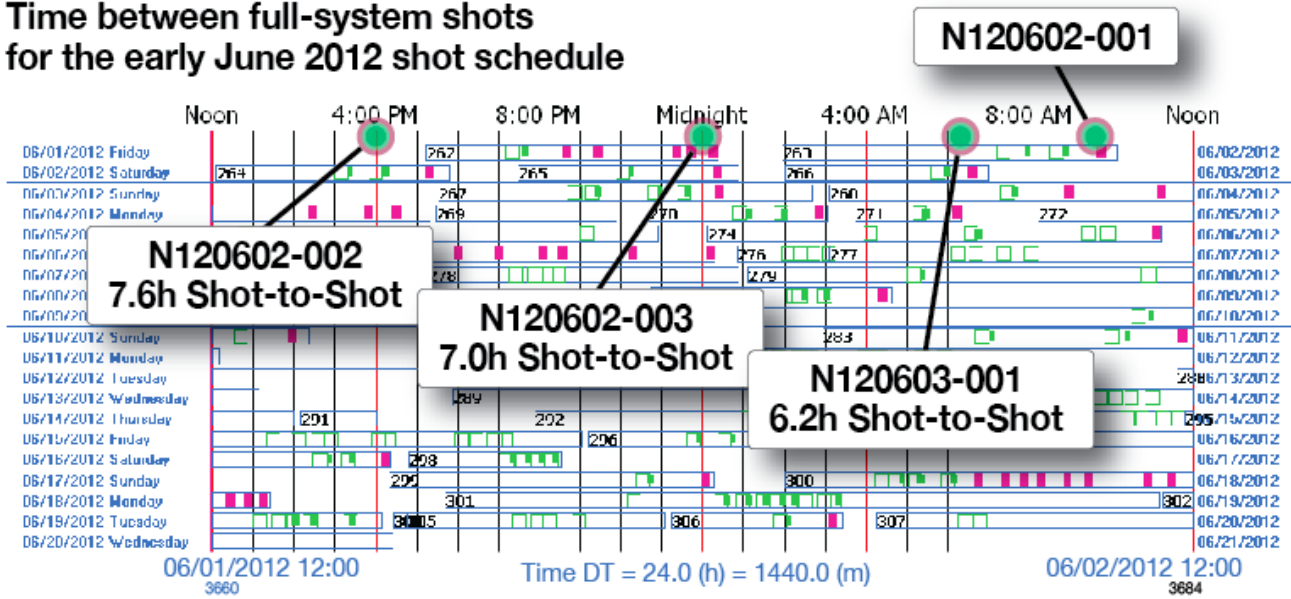


Fig. 32. An example of turnaround time between full-system facility shots that occurred during June of 2012, illustrating the ability of the laser to meet its cycle-time requirement.

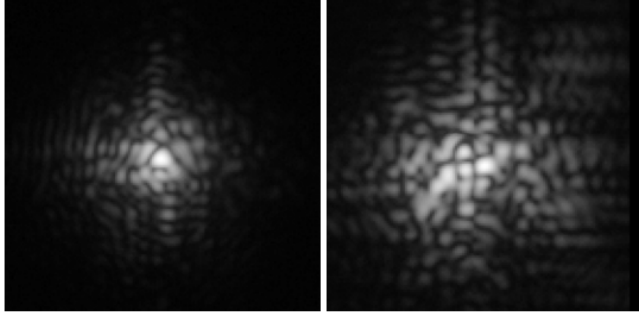


Fig. 33. Focal-spot-size measurement taken for the Beamlet laser for the first and third shots of the day with a total time separation of 4.25 hours. This illustrates the impact of heating of the laser slabs by previous shots. Beamlet had lower gas flow in the flashlamp cavity, no flow in the slab cavity, and a much lower quality deformable mirror than NIF.

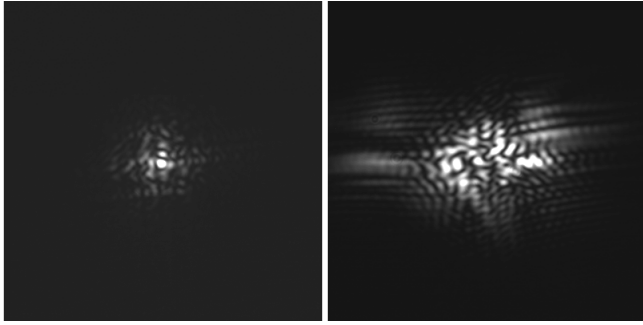


Fig. 34. Focal-spot-size measurements taken for NIF with and without the deformable mirror loop operational.



Fig. 35. Plumbing for the clean-dry air that cools the flashlamp and laser amplifier slabs between each laser shot. For sizing, note that in this photograph there is a person behind one of the pipes.

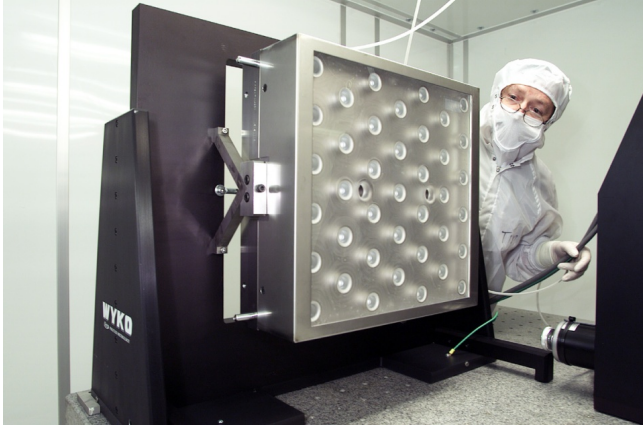


Fig. 36. Laser Mirror 1 showing its 39 actuators. Although this mirror is highly reflective at  $1.053 \mu\text{m}$ , as seen here, it is transparent in the visible.

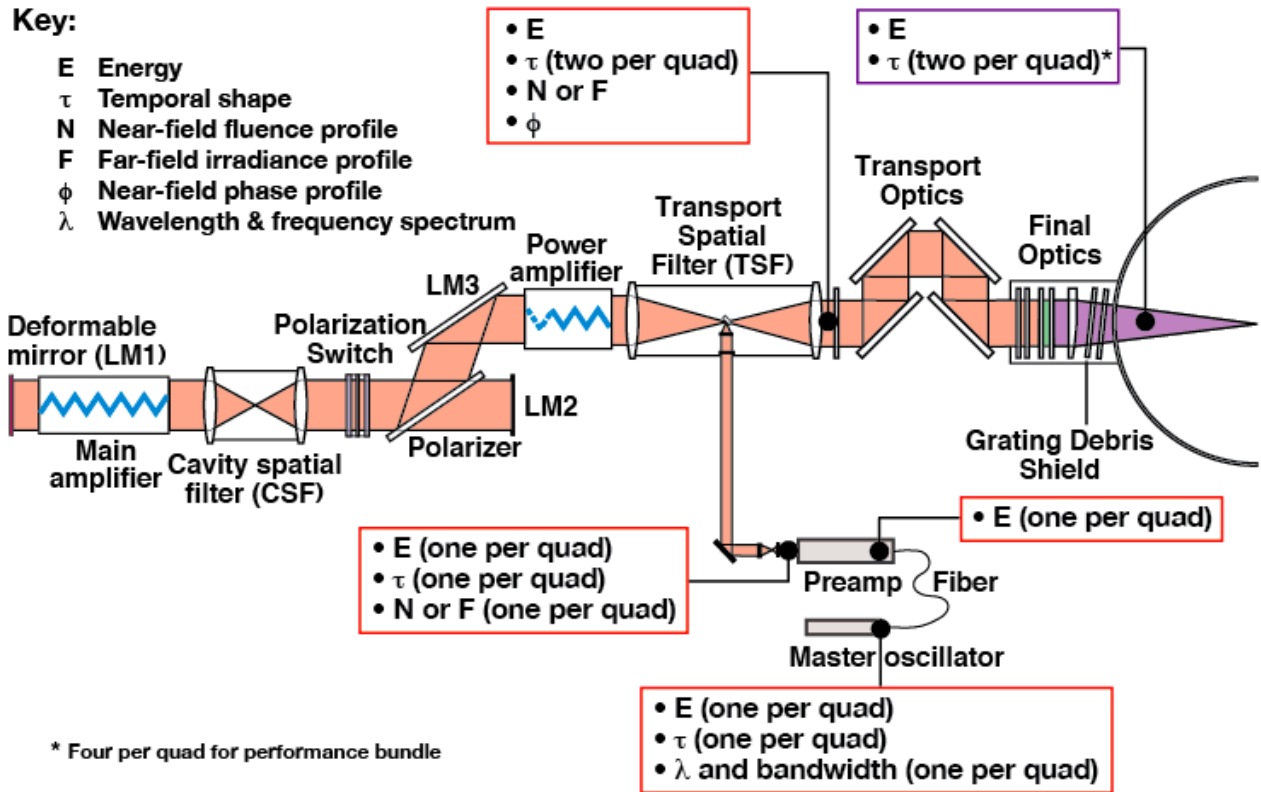


Fig. 37. Laser pulse diagnostics of NIF, presented on an annotated version of the schematic of the laser beamline.

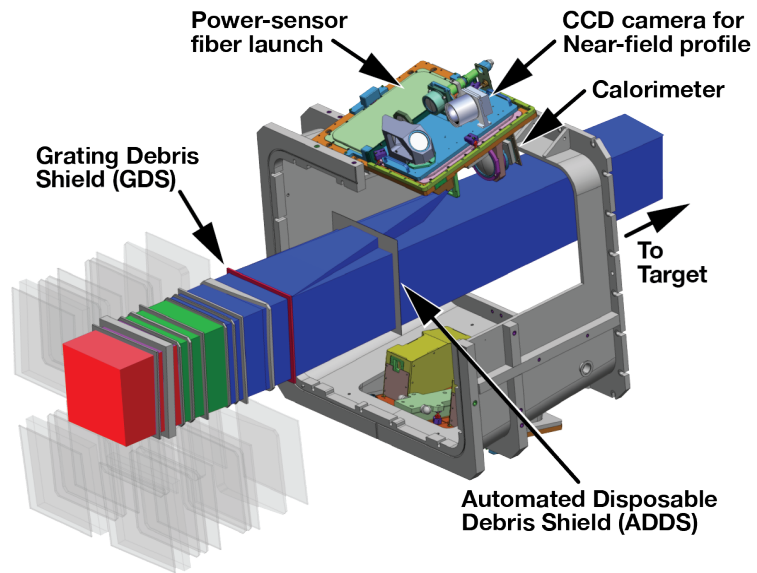


Fig. 38. Location of the Drive Diagnostics (DrD) package with respect to the Final Optics Assembly (FOA) and the target. The optics and beams in one Integrated Optics Module (IOM) are highlighted while optics of the other three IOMs are ghosted in.

## References

---

1. J. T. HUNT, K. R. MANES, J. R. MURRAY, P. A. RENARD, R. SAWICKI, J. B. TRENHOLME, and W. WILLIAMS, "Laser Design Basis for the National Ignition Facility," UCRL-JC-117399, NTIS # DE94016700, OSTI ID# 10173650, *Fusion Technology*, **26**, 767 (1994).
2. R.W. PATTERSON to S.L. SAMUELSON, "NIF Functional Requirements and Primary Criteria, Rev. 1.8," NIF-0001006-OE, Lawrence Livermore National Laboratory (LLNL) (Sept 2006). NIF-0001006-OE, LLNL-TR-661755
3. O. A. HURRICANE, D. A. CALLAHAN, D. T. CASEY, P. M. CELLIERS, C. CERJAN, E. L. DEWALD, T. R. DITTRICH, T. DÖPPNER, D. E. HINKEL, L. F. BERZAK HOPKINS, J. L. KLINE, S. LE PAPE, T. MA, A. G. MACPHEE, J. L. MILOVICH, A. PAK, H. S. PARK, P. K. PATEL, B. A. REMINGTON, J. D. SALMONSON, P. T. SPRINGER, and R. TOMMASINI, "Fuel Gain Exceeding Unity in an Inertially Confined Fusion Implosion," *Nature*, **506**, 343 (2014), doi:10.1038/nature13008, <http://www.nature.com/nature/journal/v506/n7488/full/nature13008.html> (published online 12 February 2014).
4. J. A. PAISNER to S. L. SAMUELSON, "Project Completion Criteria, Needs," LLNL-TR-662136, LLNL, (1997).
5. E. I. MOSES, J. ATHERTON, L. LAGIN, D. LARSON, C. KEANE, B. MACGOWAN, R. PATTERSON, M. SPAETH, B. VAN WONTERGHEM, P. WEGNER, and R. KAUFFMAN, "The National Ignition Facility: Transition to a User Facility," submitted to IOP Conference Series (IFSA 2013).

- 
6. C. A. HAYNAM, P. J. WEGNER, J. M. AUERBACH, M. W. BOWERS, S. N. DIXIT, G. V. ERBERT, G. M. HEESTAND, M. A. HENESIAN, M. R. HERMANN, K. S. JANCAITIS, K. R. MANES, C. D. MARSHALL, N. C. MEHTA, J. MENAPACE, E. MOSES, J. R. MURRAY, M. C. NOSTRAND, C. D. ORTH, R. PATTERSON, R. A. SACKS, M. J. SHAW, M. SPAETH, S. B. SUTTON, W. H. WILLIAMS, C. C. WIDMAYER, R. K. WHITE, S. T. YANG, and B. M. VANWONTERGHEM, "National Ignition Facility Laser Performance Status," *Appl. Opt.*, **46**, 3276 (2007).
  7. C. A. HAYNAM, Ed., "Summary of the Evidence File Demonstrating Completion of the NIF Project Completion Criteria (PCC)", LLNL-TR-665560, LLNL (Jan 2009).
  8. P. A. ARNOLD, S. D. HULSEY, G. T. ULLERY, D. E. PETERSEN, C. W. OLLIS, M. A. NEWTON, T. B. HARWELL, and L. M. HADOVSKI, "An Update on the Status of the NIF Power Conditioning System," *IEEE Trans. Plasma Sci.*, **36**, 383 (April 2008).
  9. P. A. ARNOLD, G. F. JAMES, D. E. PETERSEN, D. L. PENDLETON, G. B. MCHALE, F. BARBOSA, A. S. RUNTAL, and P. L. STRATTON, "An Update on NIF Pulsed Power," *IEEE*, 978-1-4244-4065-8/09, 352 (2009).
  10. W. W. SIMMONS, J. T. HUNT, and W. E. WARREN, "Light Propagation through Large Laser Systems," *IEEE Journal of Quantum Electronics*, **QE-17**, 9, 1727 (Sept 1981).
  11. J. R. MURRAY, J. R. SMITH, R. B. EHRLICH, D. T. KYRAZIS, C. E. THOMPSON, T. L. WEILAND, and R. B. WILCOX, "Experimental Observation and Suppression of Transverse Brillouin Scattering in Large Optical Components," *JOSA B*, **6**,12, 2402 (Dec 1989).
  12. M. A. HENESIAN, C. D. SWIFT, and J. R. MURRAY, "Stimulated Rotational Raman Scattering in Nitrogen in Long Air Paths," *Optics Letters*, **10**, 565 (Nov 1985).

- 
13. C. W. CARR, J. B. TRENHOLME, and M. L. SPAETH, "Effect of Temporal Pulse Shape on Optical Damage," *Applied Physics Letters*, **90**, 1 (2007).
  14. K. R. MANES and W. W. SIMMONS, "Statistical Optics Applied to High-power Glass Lasers," *J. Opt. Soc. Am. A*, **2**, 4, 528 (April 1985).
  15. M. A. Norton, E. E. Donohue, M. D. Feit, R. P. Hackel, W. G. Hollingsworth, A. M. Rubenchik, M. L. Spaeth, "Growth of laser damage in SiO<sub>2</sub> under multiple wavelength irradiation," November 1, 2005, *Boulder Damage Symposium XXXVII*, Boulder, CO, United States, September 19-21, 2005, UCRL-PROC-216742, NTIS# DE2006877930, OSTI ID# 877930
  16. MARY A. NORTON, C. WREN CARR, ADRA V. CARR, EUGENE E. DONOHUE, MICHAEL D. FEIT, WILLIAM G. HOLLINGSWORTH, ZHI LIAO, RALUCA A. NEGRES, ALEXANDER M. RUBENCHIK, and P. J. WEGNER, "Laser Damage Growth in Fused Silica with Simultaneous 351 nm and 1053 nm Irradiation," *Boulder Damage Symposium*, Boulder, CO, September 22–24, 2008, LLNL-Proc-408343, LLNL, (October 2008)
  17. R. K. KIRKWOOD, B. J. MACGOWAN, D. S. MONTGOMERY, B. B. AFEYAN, W. L. KRUER, D. M. PENNINGTON, S. C. WILKS, J. D. MOODY, K. WHARTON, C. A. BACK, K. G. ESTABROOK, S. H. GLENZER, M. A. BLAIN, R. L. BERGER, D. E. HINKEL, B. F. LASINSKI, E. A. WILLIAMS, D. MUNRO, B. H. WILDE and C. ROUSSEAU, "Observation of Multiple Mechanisms for Stimulating Ion Waves in Ignition Scale Plasmas," *Phys. Plasmas*, **4**, 1800 (1997).
  18. E. A. WILLIAMS , B. I. COHEN , L. DIVOL, M. R. DORR, J. A. HITTINGER, D. E. HINKEL, A. B. LANGDON, R. K. KIRKWOOD, D. H. FROULA, and S. H. GLENZER,

- 
- “Effects of Ion Trapping on Crossed-laser-beam Stimulated Brillouin Scattering,” *Phys. Plasmas*, **11**, 231 (2004).
19. P. MICHEL, L. DIVOL, R. P. J. TOWN, M. D. ROSEN, D. A. CALLAHAN, N. B. MEEZAN, M. B. SCHNEIDER, G. A. KYRALA, J. D. MOODY, E. L. DEWALD, K. WIDMANN, E. BOND, J. L. KLINE, C. A. THOMAS, S. DIXIT, E. A. WILLIAMS, D. E. HINKEL, R. L. BERGER, O. L. LANDEN, M. J. EDWARDS, B. J. MACGOWAN, J. D. LINDL, C. HAYNAM, L. J. SUTER, S. H. GLENZER, and E. MOSES, “Three-wavelength Scheme to Optimize Hohlraum Coupling on the National Ignition Facility,” *Phys. Rev. E*, **83**, 046409 (2011).
20. D. A. Callahan, N. B. Meezan, S. H. Glenzer, A. J. MacKinnon, L. R. Benedetti, D. K. Bradley, J. R. Celeste, P. M. Celliers, S. N. Dixit, T. Doöppner, E. G. Dzentitis, S. Glenn, S. W. Haan, C. A. Haynam, D. G. Hicks, D. E. Hinkel, O. S. Jones, O. L. Landen, R. A. London, A. G. MacPhee, P. A. Michel, J. D. Moody, J. E. Ralph, H. F. Robey, M. D. Rosen, M. B. Schneider, D. J. Strozzi, L. J. Suter, R. P. J. Town, K. Widmann, E. A. Williams, M. J. Edwards, B. J. MacGowan, J. D. Lindl, L. J. Atherton, G. A. Kyrala, J. L. Kline, R. E. Olson, D. Edgell, S. P. Regan, A. Nikroo, H. Wilkins, J. D. Kilkenny, and A. S. Moore, “The velocity campaign for ignition on NIF”, *Physics of Plasmas* (1994-present) **19**, 056305 (2012); doi: 10.1063/1.3694840
21. S. Sommer, E. Bliss, “Section 11. Beam positioning” of *NIF Laser System Performance Ratings*, UCRL-ID-131115, July (1998) UCRL-ID-131115, Supplement to Proceedings of SPIE, V 3492, Third International Conf on Solid State Lasers for Application to Inertial Confinement Fusion

- 
22. S. C. BURKHART, E. BLISS, P. DI NICOLA, D. KALANTAR, R. LOWE-WEBB, T. MCCARVILLE, D. NELSON, T. SALMON, T. SCHINDLER, J. VILLANUEVA, and K. WILHELMSSEN, "National Ignition Facility System Alignment," *Applied Optics*, **50**, 8, 1136 (March 10, 2011).
  23. C. VANN, "SixDOF Sensor Improves Manufacturing Flexibility", LLNL Science & Technology Review, pp 21, October 1996, R&D Magazine (preprint), UCRL-JC-123658 (Mar 1996).
  24. P. DI NICOLA, D. KALANTAR, T. MCCARVILLE, J. KLINGMANN, S. ALVAREZ, R. LOWE-WEBB, J. LAWSON, P. DATTE, P. DANFORTH, M. SCHNEIDER, J-M. DI NICOLA, J. JACKSON, C. ORTH, S. AZEVEDO, R. TOMMASINI, A. MANUEL, and R. WALLACE, "Beam and Target Alignment at the National Ignition Facility Using the Target Alignment Sensor (TAS)," *Proc. of SPIE*, **8505**, 85050B (Oct 2012).
  25. D. EIMERL, J. ROTHERNBERG, M. KEY, S. WEBER, C. VERDON, S. SKUPSKY, J. SOURES, and S. CRAXTON, "Configuring NIF for Direct Drive Experiments", UCRL-JC-121271, NTIS# DE96000094, Submitted to 1st Annual International Conference on Solid-State Lasers for Application to Inertial Confinement Fusion, Monterey, CA May 30 - June 2, 1995, (July, 11, 1995)
  26. R. MORE, Retired LLNL, Re: Possible origin of laser pre-pulse, Personal Communication October (2011).
  27. J. P. LEIDINGER, French Commissariat à l'Energie Atomique (CEA), France, Re: Residual 1w light could be scattered by dirty debris shield or aging optics into the region of the LEH, Personal Communication LLNL-CEA VTC (12/2012), and C.A. THOMAS,

- 
- LLNL, Re: Scattering of light into the LEH to lead to pre-pulse, Personal Communication, 2012.
28. J. P. LEIDINGER, French Commissariat à l’Energie Atomique (CEA), France, Personal Communication re: “It was recognized in 2013 that the NIF VISAR diagnostic. .... Could be used as a time-dependent monitor of the integrity of the Al layer...”, Conclusion viewgraph from LLNL-CEA VTC (12/2013)»
29. P. M. CELLIERS, D. K. BRADLEY, G. W. COLLINS, D. G. HICKS, T. R. BOEHLY, and W. J. ARMSTRONG, “Line-imaging Velocimeter for Shock Diagnostics at the OMEGA Laser Facility,” UCRL-JRNL-202213, *Rev Sci. Instrum.*, **75**, 4916 (2004).
30. H. F. ROBEY, P. M. CELLIERS, J. L. KLINE, A. J. MACKINNON, T. R. BOEHLY, O. L. LANDEN, J. H. EGGERT, D. HICKS, S. LE PAPE, D. R. FARLEY, M. W. BOWERS, K. G. KRAUTER, D. H. MUNRO, O. S. JONES, J. L. MILOVICH, D. CLARK, B. K. SPEARS, R. P. J. TOWN, S. W. HAAN, S. DIXIT, M. B. SCHNEIDER, E. L. DEWALD, K. WIDMANN, J. D. MOODY, T. D. DÖPPNER, H. B. RADOUSKY, A. NIKROO, J. J. KROLL, A. V. HAMZA, J. B. HORNER, S. D. BHANDARKAR, E. DZENITIS, E. ALGER, E. GIRALDEZ, C. CASTRO, K. MORENO, C. HAYNAM, K. N. LAFORTUNE, C. WIDMAYER, M. SHAW, K. JANCAITIS, T. PARHAM, D. M. HOLUNGA, C. F. WALTERS, B. HAID, T. MALSBUY, D. TRUMMER, K. R. COFFEE, B. BURR, L. V. BERZINS, C. CHOATE, S. J. BRERETON, S. AZEVEDO, H. CHANDRASEKARAN, S. GLENZER, J. A. CAGGIANO, J. P. KNAUER, J. A. FRENJE, D. T. CASEY, M. GATU JOHNSON, F. H. SÉGUIN, B. K. YOUNG, M. J. EDWARDS, B. M. VAN WONTERGHEM, J. KILKENNY, B. J. MACGOWAN,

- 
- J. ATHERTON, J. D. LINDL, D. D. MEYERHOFER, and E. MOSES, "Precision Shock Tuning on the National Ignition Facility," *Phys. Rev. Lett.*, **108**, 215004 (2012).
31. R. P. J. TOWN, D. K. BRADLEY, A. KRITCHER, O. S. JONES, J. R. RYGG, R. TOMMASINI, M. BARRIOS, L. R. BENEDETTI, L. F. BERZAK HOPKINS, P. M. CELLIERS, T. DÖPPNER, E. L. DEWALD, D. C. EDER, J. E. FIELD, S. M. GLENN, N. IZUMI, S. W. HAAN, S. F. KHAN, J. L. KLINE, G. A. KYRALA, T. MA, J. L. MILOVICH, J. D. MOODY, S. R. NAGEL, A. PAK, J. L. PETERSON, H. F. ROBEY, J. S. ROSS, R. H. H. SCOTT, B. K. SPEARS, M. J. EDWARDS, J. D. KILKENNY and O. L. LANDEN, "Dynamic Symmetry of Indirectly Driven Inertial Confinement Fusion Capsules on the National Ignition Facility," *Phys. Plasmas*, **21**, 056313 (2014).
32. O. L. LANDEN, R. BENEDETTI, D. BLEUEL, T. R. BOEHLY, D. K. BRADLEY, J. A. CAGGIANO, D. A. CALLAHAN, P. M. CELLIERS, C. J. CERJAN, D. CLARK, G. W. COLLINS, E. L. DEWALD, S. N. DIXIT, T. DOEPPNER, D. EDGELL, J. EGGERT, D. FARLEY, J. A. FRENJE, V. GLEBOV, S. M. GLENN, S. H. GLENZER, S. W. HAAN, A. HAMZA, B. A. HAMMEL, C. A. HAYNAM, J. H. HAMMER, R. F. HEETER, H. W. HERRMANN, D. G. HICKS, D. E. HINKEL, N. IZUMI, M. GATU JOHNSON, O. S. JONES, D. H. KALANTAR, R. L. KAUFFMAN, J. D. KILKENNY, J. L. KLINE, J. P. KNAUER, J. A. KOCH, G. A. KYRALA, K. LAFORTUNE, T. MA, A. J. MACKINNON, A. J. MACPHEE, E. MAPOLES, J. L. MILOVICH, J. D. MOODY, N. B. MEEZAN, P. MICHEL, A. S. MOORE, D. H. MUNRO, A. NIKROO, R. E. OLSON, K. OPACHICH, A. PAK, T. PARHAM, P. PATEL, H. S. PARK, R. P. PETRASSO, J. RALPH, S. P. REGAN, B. A. REMINGTON, H. G. RINDERKNECHT, H. F. ROBEY, M. D. ROSEN, J. S. ROSS, J. D. SALMONSON, T. C. SANGSTER, M. B. SCHNEIDER, V. SMALYUK,

- 
- B. K. SPEARS, P. T. SPRINGER, L. J. SUTER, C. A. THOMAS, R. P. J. TOWN, S. V. WEBER, P. J. WEGNER, D. C. WILSON, K. WIDMANN, C. YEAMANS, A. ZYLSTRA, M. J. EDWARDS, J. D. LINDL, L. J. ATHERTON, W. W. HSING, B. J. MACGOWAN, B. M. VAN WONTERGHEM, and E. I. MOSES, "Progress in the Indirect-drive National Ignition Campaign," *Plasma Phys. Control. Fusion*, **54**, 124026 (2012).
33. JM DI NICOLA, S. YANG, S.DIXIT at al., LLNL, Personal Communication re: More detailed analysis of the unconverted  $1\omega$  light ... measurements now with an active sensor at TCC ... had shown that it is important to consider pre-pulse signal as the both of both  $3\omega$  and  $1\omega$  sources of light, NIF Pre-Pulse Update LLNL-CEA VTC (11/2013)
34. J. D. LINDL, P. AMENDT, R. L. BERGER, S. G. GLENDINNING, S. H. GLENZER, S. W. HAAN, R. L. KAUFFMAN, O. L. LANDEN, AND L. J. SUTER, "The Physics Basis for Ignition using Indirect Drive Targets on the NIF," *Phys Plasmas*, **11**, 340 (2004).
35. JOSEPH A. MENAPACE, FRANCOIS Y. GENIN, WAYNE F. BROCIOSUS, "Magnetorheological Finishing for Imprinting Continuous-phase Plate Structures onto Optical Surfaces," UCRL-CONF-I 53850, *Proc. SPIE 5273*, Laser-Induced Damage in Optical Materials: 2003, 220 (June 10, 2004), doi:10.1117/12.527822.
36. S. SKUPSKY, R. W. SHORT, T. KESSLER, R. S. CRAXTON, S. LETZRING, and J. M. SOURES, "Improved Laser Beam Uniformity Using the Angular Dispersion of Frequency-Modulated Light," *J. Appl. Phys.*, **66**, 3456 (1989).
37. H. T. POWELL, S. N. DIXIT, and M. A. HENESIAN, "Beam Smoothing Capability on the Nova Laser," UCRL-LR-105821-91-1, *Inertial Confinement Fusion*, **1**, 1, 28 (1990).

- 
38. S. N. DIXIT, D. MUNRO, J. R. MURRAY, M. NOSTRAND, P. J. WEGNER, D. FROULA, C. A. HAYNAM, and B. J. MACGOWAN, “Polarization Smoothing on the National Ignition Facility,” *J. Phys. IV France*, **133**, 717 (June 2006).
  39. STEVE SUTTON, CHRIS MARSHALL, and CHRIS HAYNAM, “Results of the NEL Shot-Rate Campaign,” LLNL-TR-661898, LLNL (Jan 2004).
  40. G. ERBERT, “Wavelength-Stability Measurement,” 2005 to 2006, (unpublished work of one of the authors).